

A Quarkyonic Quark-Meson Coupling Model for Nuclear and Neutron Matter

Koichi Saito*

*Department of Physics and Astronomy,
Tokyo University of Science, Noda 278-8510, Japan*

Tsuyoshi Miyatsu[†] and Myung-Ki Cheoun[‡]

*Department of Physics and OMEG Institute,
Soongsil University, Seoul 06978, Republic of Korea*

(Dated: December 5, 2025)

Abstract

We unite the dual quarkyonic model with the quark-meson coupling (QMC) model to construct a novel nuclear model based on the quark degrees of freedom, which can cover a wide range of nuclear density from low density to the crossover region. In the model, the relativistic, gaussian quark wavefunction is used to describe the nucleon structure. We first evaluate the energy density, chemical potential, pressure and sound velocity within the ideal Fermi gas picture. In this case, those physical quantities are discontinuous or divergent at the quark saturation density, where quarkyonic phase emerges. To remove such singular behavior, we next introduce an infrared regulator, and combine the dual quarkyonic model and the QMC model to include the nuclear interaction – we call it the quarkyonic quark-meson coupling (QQMC) model. We then find that the quark saturation density depends strongly on the nucleon size. For example, when $r_p = 0.6$ (0.8) fm, where r_p is the root-mean-square radius of proton, the quark saturation density is about 3.6 (1.5) $\times \rho_0$ in symmetric nuclear matter, where ρ_0 is the nuclear saturation density. It is notable that the nuclear interaction is quite important to consider physical quantities quantitatively. In fact, the QQMC model can produce the sound velocity which is consistent with that inferred from the observed data of several neutron stars. Furthermore, pressure in symmetric or pure neutron matter deduced from the experiments of heavy-ion collisions at high energy can be explained by the QQMC model as well. We discuss in detail the formulation for the QQMC model and the physical quantities calculated by the model.

* koichi.saito@rs.tus.ac.jp

† tsuyoshi.miyatsu@ssu.ac.kr

‡ cheoun@ssu.ac.kr

I. INTRODUCTION AND PRERIMINARIES

For more than a decade, the masses and radii of neutron stars (NSs), together with the constraint on the tidal deformability from the binary neutron-star merger event, GW170817 [1–3], have been receiving much attention theoretically as well as experimentally, because these observations can provide decisive tests for understanding the equations of state (EoSs) for cold, dense nuclear matter. In particular, members of the neutron-star population with the heaviest masses are quite important, because, from them, we can obtain information on baryonic and/or exotic compositions in EoSs, which is not accessible through terrestrial experiments. The observed heavy pulsars are listed as [4]: PSR J1614–2230 ($M_P \sim 1.91M_\odot$) [5], PSR J0348+0432 ($M_P \sim 2.01M_\odot$) [6], PSR J0740+6620 ($M_P \sim 2.08M_\odot$) [7], and PSR J0952–0607 ($M_P \sim 2.35M_\odot$) [8], where $M_P (M_\odot)$ is the mass of pulsar (sun). Furthermore, the precise measurements of NS radii have been performed with the NICER telescope observation [9–13].

One of the interesting findings from the NS observations concerns the stiffness of NS matter. As the nuclear density, ρ_N , increases, conventional nuclear calculations usually lead to a *softening* of EoS for NS matter, because new degrees of freedom like hyperons etc. are opened at high densities. However, the result from NS observations tells us that the EoS is rapidly *stiffened* slightly above the nuclear saturation density, ρ_0 . This discrepancy is called *the hyperon puzzle*, and a tremendous amount of research in this field has been reported, see, for example, Refs. [14–17].

Among those various approaches, the idea of quarkyonic matter, which is originally based on the $1/N_c$ expansion [18] and hadron-quark continuity [19, 20], seems one of the promising ways to settle the hyperon puzzle. For review and recent developments, see Refs. [21–23].

In particular, Fujimoto et al. [24, 25] have recently constructed a novel model of quarkyonic matter, which is called the ideal dual quarkyonic (IdylliQ) model. See also Ref. [26]. It is a dual model, i.e. the matter may either be viewed in terms of nucleon degrees of freedom or as quarks, made from free nucleons which are only subject to the Pauli exclusion principle of the nucleons and of the quarks inside the nucleon. In the IdylliQ model, the nucleon is composed of quarks whose quark momentum distribution, $\varphi(q)$, is supposed to be a Yukawa-type function

$$\varphi(\mathbf{q}) = \frac{2\pi^2}{\Lambda^3} \frac{e^{-q/\Lambda}}{q/\Lambda}, \quad (1)$$

with the typical momentum scale $\Lambda \sim \Lambda_{\text{QCD}}$. This choice allows us to solve the IdylliQ model exactly. Then, the collecting quark contributions from each nucleon generates the quark distribution in nuclear matter. For symmetric nuclear matter, it is described by the simple sum rule (or duality relation)

$$f_Q(q) = \int_k \varphi\left(\mathbf{q} - \frac{\mathbf{k}}{N_c}\right) f_N(k), \quad (2)$$

where $\int_k \equiv \int d^3\mathbf{k}/(2\pi)^3$, $f_N(k)$ [$f_Q(q)$] is the momentum-space distribution of nucleon [quark Q (= up (u) or down (d))] with Fermi statistics, $0 \leq f_N(k), f_Q(q) \leq 1$, and N_c is the number of color. Hereafter, the letters q and k are used exclusively for quarks and nucleons, respectively.

At low density, the matter is best viewed in terms of only nucleons. However, as ρ_N grows up, the probability f_Q increases and eventually reaches the upper bound, i.e. $f_Q(q) = 1$ at $q = 0$. Above such density, the low momentum states of the quarks are fully occupied, i.e. *the quark saturation* occurs, and the matter turns out to be quarkyonic matter from ordinary nuclear matter. We call this density the quark saturation density, ρ_{sat} , and such phase may be recognized as *the soft deconfinement* region [20]. As a consequence, the dual nucleon momentum distribution in symmetric nuclear matter is separated into two segments

$$f_N(k) = \frac{1}{N_c^3} \theta(k_b - k) + \theta(k_s - k) \theta(k - k_b), \quad (3)$$

which is the order of $1/N_c^3$ in the *bulk* Fermi sea ($k \leq k_b$) while forms the nucleon *shell* structure at $k_b \leq k \leq k_s$. Due to the Pauli blocking at the quark level, this shape is energetically more favorable than in the ordinary shell structure. This fact realizes that, above the quark saturation density, pressure, P , and the sound velocity, v_s , are enhanced considerably.

In Ref. [25], expanding this idea to the matter including hyperon degrees of freedom, the important effect of the quark substructure in neutron matter is investigated, that is, above the quark saturation density, the onset of hyperon is shifted to higher density, because the phase space of d quarks are already preoccupied by neutrons, which prevents the appearance of hyperons involving d quark, especially Λ and Σ with $S = -1$. Thus, in quarkyonic matter, the softening in EoS stemming from new degrees of freedom of hyperons is hindered until the threshold of the cascade Ξ^0 with $S = -2$, which does not contain any d quark, opens. This story may give a natural, robust answer to the hyperon puzzle.

However, it is urgently desirable to consider the effect of interactions among baryons to make the quarkyonic model more realistic. In Ref. [27], Koch et al. have first performed such investigation using the IdylliQ model with the interaction due to σ and π meson exchanges, and have studied the possibility that normal nuclear matter is quarkyonic. In their calculation, the onset density of quarkyonic matter is below ρ_0 , and they have argued that the strong depletion of nucleons at low momentum generated by the quark Pauli blocking is consistent with the experimental data of quasi-elastic electron scattering off nuclei. See also Ref. [28]. It is also vital to examine whether such depletion is again consistent with the EMC (European Muon Collaboration) effect [29, 30] and other nuclear reactions like a single-nucleon knockout [31]. In any case, it is *quite remarkable* that the explicit quark degrees of freedom may play a pivotal role in nuclear medium around the nuclear saturation density, ρ_0 .

On the other hand, even below ρ_0 , using the quark-meson coupling (QMC) model, it has been indicated that subhadronic degrees of freedom are essential to understand the properties of nuclear medium and finite nuclei [32–34]. The QMC model is originally based on a mean field description of non-overlapping nucleon (or baryon) bags bound by the self-consistent exchange of scalar and vector mesons in the isoscalar and isovector channels [35, 36]. The model is extended to investigate the properties of finite nuclei, in which, using the Born-Oppenheimer approximation to describe the interacting quark-meson system, one can derive the effective equation of motion for the nucleon (or baryon), as well as the self-consistent equations for the meson mean fields [32, 33, 37]. In Ref. [38], using the Miller-Spencer correlation function, the short-range quark-quark correlation is introduced into the QMC model phenomenologically and it is found that the saturation curve for symmetric nuclear matter is eventually turned out stiff at high density. Furthermore, by using naive dimensional analysis, it is possible to see that the QMC model can provide remarkably natural coupling constants and hence the model itself is regarded as a natural effective field theory for nuclei [39].

The model can be applied to various finite nuclei, including strange and exotic hyper-nuclei [40, 41]. In Ref. [33], the extensive application to these topics with a discussion of similarities and differences between the QMC and Skyrme energy density functionals are presented in details. It is also of great interest that the QMC model predicts a variation of the nucleon form factors in nuclear matter [42], which affects certainly the analysis of elec-

tron scattering off nuclei [43], including the polarization-transfer in quasi-elastic $A(\vec{e}, e'\vec{p})$ reaction (A1 Collaboration) [44] and the EMC effect [45, 46].

It is remarkable that the heart of the QMC model is *the scalar polarizability* of a baryon in matter, i.e. the variation of the quark scalar density inside the nucleon caused by the condensed, scalar mean field, which can naturally describe nuclear saturation and induce many-body forces [47]. Therefore, hadrons are polarized in medium even below ρ_0 , because they have quark substructure. The medium modification of the nucleon has been examined by Lattice calculation (NPLQCD Collaboration) [48] as well.

The QMC model has been applied to the EoSs for massive NSs and the hyperon puzzle [49–51], and has predicted that, in the EoS for NS, the cascade Ξ^- first appears around $\rho_N/\rho_0 \sim 3$ and other hyperons are all suppressed until $\rho_N/\rho_0 \sim 4.5$. A more phenomenological method to include short range repulsion may be based on the excluded volume effect [52]. This method was recently used in the framework of the QMC model [53] and the NJL-type model [54].

The present paper is aimed at unifying the dual quarkyonic picture and the QMC model to construct a new nuclear model based on the quark degrees of freedom, which is valid from low density to a crossover region where the transition from baryonic to quark matter occurs. Therefore, the new model includes the effect of Pauli blocking at the quark level as well as the scalar polarizability of a nucleon in medium.

In the IdylliQ model, the single quark momentum distribution in a nucleon is chosen to be the Yukawa-type function, Eq. (1), specifically, while in the QMC model the quark wavefunction is usually given by the bag model. Therefore, it is necessary to prepare a unified setup for the quark wavefunction. In this paper, we use the gaussian wavefunction for a quark in a nucleon, which is given by the relativistic confinement potential of the scalar-vector harmonic oscillator (HO) type

$$U(r) = \frac{c}{2}(1 + \gamma_0)r^2, \quad (4)$$

with the strength parameter c . The QMC model with the relativistic HO potential is sometimes referred as the quark mean field (QMF) model [55, 56] or the modified quark-meson coupling (MQMC) model [57]. This quark model has some pleasant feature that all quantities of interest can be basically calculated analytically. For the detail, see Ref. [58].

It is well known that the Dirac equation with the HO potential, Eq. (4), can be solved

analytically [59, 60]. In free space, the lowest-state solution for a iso-symmetric ($u = d$) quark is given by

$$\psi_Q(\mathbf{r}) = \frac{1}{\pi^{3/4}a^{3/2}} \sqrt{\frac{2\lambda^2 a^2}{2\lambda^2 a^2 + 3}} \begin{pmatrix} 1 \\ i\vec{\sigma} \cdot \hat{\mathbf{r}} \frac{1}{\lambda a} \left(\frac{\mathbf{r}}{a}\right) \end{pmatrix} e^{-r^2/2a^2} \chi, \quad (5)$$

$$\lambda = \epsilon + m, \quad a^2 = \frac{1}{\sqrt{c\lambda}} = \frac{3}{\epsilon^2 - m^2}, \quad (6)$$

where m is the constituent quark mass, a is the length scale and χ is the quark spinor. Here, the single-particle quark energy, ϵ , is determined by

$$\sqrt{\epsilon + m}(\epsilon - m) = 3\sqrt{c}. \quad (7)$$

Note that, in the limit $\lambda \rightarrow \infty$, this wavefunction turns out to be the nonrelativistic (NR) one.

The zeroth-order energy of the nucleon, E_N^0 , is then simply given by a sum of the quark energies, $E_N^0 = 3\epsilon$. Now we should take into account some corrections to the nucleon energy such as the spin correlations, E_N^{spin} , due to the quark-gluon and quark-pion interactions [61, 62], and the center of mass (c.m.) correction, $E_N^{c.m.}$. Here we do not calculate the spin correlation explicitly, but we assume that it can be treated as a constant parameter which is fixed so as to reproduce the nucleon mass [55, 56]. The c.m. correction to the spurious motion can be calculated analytically [58]

$$E_N^{c.m.} = \frac{77\epsilon + 31m}{3a^2(3\epsilon + m)^2}. \quad (8)$$

The nucleon mass in vacuum is thus given by

$$M_N = E_N^0 + E_N^{spin} - E_N^{c.m.}, \quad (9)$$

which is equal to the proton or neutron mass ($M_N = M_p = M_n$), because any breaking of isospin symmetry is not included. We also find the root-mean-square charge radius of proton including the c.m. correction as [58]

$$r_p \equiv \langle r^2 \rangle_p^{1/2} = \sqrt{\frac{11\epsilon + m}{(3\epsilon + m)(\epsilon^2 - m^2)}}. \quad (10)$$

In this quark model, we have three parameters, c , m , E_N^{spin} . We then choose the quark mass as follows: case 1, $m = 250$ MeV; case 2, $m = 300$ MeV; case 3, $m = 350$ MeV. The

TABLE I. Parameters in the quark model and the quark saturation density, ρ_{sat} . The nuclear saturation density is chosen to be $\rho_0 = 0.15 \text{ fm}^{-3}$. The quark saturation density is listed in the last two columns (see Section II A 3).

| Case | m^a | r_p^a | a | c | ϵ | E_N^0 | E_N^{spin} | $E_N^{c.m.}$ | ρ_{sat}/ρ_0 | |
|------|-------|---------|-------|----------------------|------------|---------|--------------|--------------|---------------------|-------|
| | (MeV) | (fm) | (fm) | (fm^{-3}) | | (MeV) | | | SNM | PNM |
| 1 | 250 | 0.6 | 0.567 | 2.121 | 653.0 | 1959.1 | -539.2 | 480.9 | 4.373 | 3.371 |
| | | 0.7 | 0.665 | 1.230 | 571.8 | 1715.3 | -382.5 | 393.8 | 2.648 | 2.041 |
| | | 0.8 | 0.764 | 0.761 | 512.7 | 1538.2 | -270.3 | 328.9 | 1.714 | 1.321 |
| | | 0.9 | 0.863 | 0.496 | 468.4 | 1405.2 | -187.4 | 278.8 | 1.167 | 0.900 |
| | | 1.0 | 0.963 | 0.336 | 434.2 | 1302.7 | -124.4 | 239.3 | 0.828 | 0.638 |
| 2 | 300 | 0.6 | 0.570 | 1.923 | 670.2 | 2010.5 | -616.3 | 455.2 | 4.175 | 3.219 |
| | | 0.7 | 0.669 | 1.102 | 592.3 | 1776.8 | -468.9 | 368.8 | 2.526 | 1.947 |
| | | 0.8 | 0.769 | 0.675 | 536.3 | 1608.8 | -365.0 | 304.8 | 1.634 | 1.260 |
| | | 0.9 | 0.869 | 0.436 | 494.7 | 1484.0 | -289.1 | 255.9 | 1.114 | 0.859 |
| | | 1.0 | 0.969 | 0.293 | 463.0 | 1388.9 | -232.2 | 217.7 | 0.791 | 0.610 |
| 3 | 350 | 0.6 | 0.574 | 1.750 | 691.0 | 2072.9 | -703.6 | 430.3 | 4.010 | 3.092 |
| | | 0.7 | 0.673 | 0.993 | 616.6 | 1849.7 | -565.6 | 345.1 | 2.427 | 1.871 |
| | | 0.8 | 0.774 | 0.603 | 563.7 | 1691.1 | -469.6 | 282.5 | 1.571 | 1.212 |
| | | 0.9 | 0.874 | 0.387 | 524.8 | 1574.5 | -400.3 | 235.2 | 1.073 | 0.828 |
| | | 1.0 | 0.975 | 0.259 | 495.5 | 1486.4 | -348.8 | 198.6 | 0.764 | 0.589 |

^a Input

remaining two parameters, c , E_N^{spin} , are determined so as to reproduce the proton charge radius, $r_p = 0.6, 0.7, 0.8, 0.9, 1.0 \text{ fm}$ (the experimental value is 0.841 fm [63]), and the nucleon mass, $M_N = 939 \text{ MeV}$. In Table I, the parameters and the quark energies are summarized.

Using the gaussian quark wavefunction, Eq.(5), the single quark momentum distribution in a single nucleon is calculated as

$$\varphi(\mathbf{q}) = \pi^{3/2} a^3 \left(\frac{16\lambda^2 a^2}{2\lambda^2 a^2 + 3} \right) \left(1 + \frac{q^2}{\lambda^2} \right) e^{-a^2 q^2}, \quad (11)$$

where the second term in the right-hand side comes from the lower component of the quark

wavefunction. This satisfies the normalization condition, $\int_q \varphi(\mathbf{q}) = 1$. Through the present paper, we use this single quark momentum distribution.

In this work, in Sec. II, using the gaussian quark wavefunction, we first study the quarkyonic matter in ideal Fermi gas. We discuss the feature of the gaussian quarkyonic model, and calculate the energy density, chemical potential, pressure and sound velocity in symmetric or pure neutron matter. Furthermore, we consider a minimal correction to the gaussian quarkyonic model to remove the singular behavior at the quark saturation density. In Sec. III, we briefly review the quark-meson coupling model with a harmonic oscillator potential, and build a new, quark-based nuclear model, in which we incorporate the QMC model and the gaussian quarkyonic model. We then discuss the results of the present model in detail. Lastly, in Sec. IV, we give our summary and discussion. In Appendix A, we apply Sommerfeld expansion to the gaussian quarkyonic model.

II. QUARKYONIC MATTER IN IDEAL FERMI GAS

In this section, we study a quarkyonic model with the relativistic, gaussian quark wavefunction. We here neglect the nuclear interaction, but consider the effect of Pauli blocking at the quark level only. We call it the gaussian quarkyonic (GQ) model. Using the GQ model, we calculate several physical quantities in symmetric nuclear matter (SNM) and in pure neutron matter (PNM).

A. Gaussian quarkyonic model

In the dual quarkyonic model, the nuclear density, ρ_N , and the energy density, ϵ_N , are expressed by either the nucleon or quark momentum distribution ($f_N(k)$ or $f_Q(q)$):

$$\rho_N = \gamma \int_k f_N(k) = \gamma \int_q f_Q(q), \quad (12)$$

$$\epsilon_N[f_N] = \epsilon_Q[f_Q], \quad \epsilon_N[f_N] = \gamma \int_k E_N(k) f_N(k), \quad \epsilon_Q[f_Q] = \gamma \int_q E_Q(q) [N_c f_Q(q)], \quad (13)$$

with γ the spin-isospin degeneracy, E_N the nucleon energy, and E_Q the quark energy. This duality is ensured by the sum rule, Eq. (2). Then, it is necessary to minimize the energy density by optimizing the distributions $f_N(k)$ and $f_Q(q)$ under the constraints of Fermi statistics and the sum rule. As the sum rule is the *global* relation, i.e. f_Q is a functional of f_N , this problem is generally difficult. However, in the IdylliQ model, because the sum rule can be transformed into the *local* relation by assuming the Yukawa-type, single quark momentum distribution, the exact solutions for f_N and f_Q can be obtained analytically. In contrast, in case of the gaussian quark wavefunction, the problem is more complex, and no explicit theoretical method has been established. Thus, in this paper, we shall consider a dual quarkyonic model with the gaussian quark wavefunction *intuitively*. Further rigorous investigation on this issue is necessary in the future.

1. Nuclear density

The nuclear density, $\rho_{N(n)}$, in SNM (PNM) is expressed by

$$\rho_N = \frac{2}{\pi^2} \int dk k^2 f_N(k), \quad (14)$$

$$\rho_n = \frac{1}{\pi^2} \int dk k^2 f_n(k). \quad (15)$$

Here, we define $f_N(k) \equiv f_p(k) = f_n(k)$ for SNM, where $f_{p(n)}(k)$ is the momentum distribution for protons (neutrons). The nuclear density is also described in terms of the quark momentum distribution f_Q as in Eq.(12).

2. Presaturation region

Because, below the quark saturation density, the nuclear matter is normal, the two momentum distributions in Eqs. (14) and (15) are simply given by the usual Fermi distribution

$$f_N(k) = f_n(k) = \theta(k_s - k), \quad (16)$$

where $k_s = k_F$ (k_F the Fermi momentum).

In SNM, the dual momentum-space distribution for iso-symmetric light quarks with a given color is expressed by the sum rule (see Eq. (2))

$$f_Q(q, k_s) = \int_k \varphi \left(\mathbf{q} - \frac{\mathbf{k}}{N_c} \right) f_N(k), \quad (17)$$

which is less than unity. Then, we can calculate f_Q analytically:

$$\begin{aligned} f_Q(q, k_s) = \frac{N_c^3}{\sqrt{\pi}} & \left[\text{Er}(\bar{q}) + \text{Er}(-\bar{q}) - \text{Er}(\bar{k}_s + \bar{q}) - \text{Er}(\bar{k}_s - \bar{q}) \right. \\ & \left. + \frac{1}{2\bar{q}} \left(1 + \frac{2\bar{k}_s^2 + 1}{2\bar{\lambda}^2 + 3} \right) \left(e^{-(\bar{k}_s + \bar{q})^2} - e^{-(\bar{k}_s - \bar{q})^2} \right) + \frac{\bar{k}_s}{2\bar{\lambda}^2 + 3} \left(e^{-(\bar{k}_s + \bar{q})^2} + e^{-(\bar{k}_s - \bar{q})^2} \right) \right] \end{aligned} \quad (18)$$

where $\bar{q} \equiv aq$, $\bar{\lambda} \equiv a\lambda$, and $\bar{k} \equiv ak/N_c$ are dimensionless variables. We here define the error function as

$$\text{Er}(x) \equiv \int_x^\infty dt e^{-t^2}. \quad (19)$$

In contrast, in PNM, there are only neutrons (udd) in matter, and so the saturation of d quark first occurs because the u quark levels are half-occupied compared with the d quark

levels. Therefore, the sum rule for PNM reads [25]

$$f_d(q, k_s) = \frac{2}{3} \int_k \varphi \left(\mathbf{q} - \frac{\mathbf{k}}{N_c} \right) f_n(k), \quad (20)$$

where the factor $2/3$ is the baryon number of d quarks in a neutron. It can be calculated analytically as well.

3. At quark saturation density

At quark saturation density, the quark momentum distribution reaches unity at $q = 0$. In SNM, the nucleon momentum k_{sat} at ρ_{sat} is given by the saturation condition

$$g_Q(k_{sat}) = \frac{N_c^3}{\sqrt{\pi}} \left[\sqrt{\pi} - 2\text{Er}(\bar{k}_{sat}) - 2\bar{k}_{sat} \left(1 + \frac{2\bar{k}_{sat}^2}{2\bar{\lambda}^2 + 3} \right) e^{-\bar{k}_{sat}^2} \right] = 1, \quad (21)$$

where we define $g_Q(k) \equiv f_Q(0, k)$. Similarly, in PNM, the neutron momentum k_{sat} at ρ_{sat} is calculated by

$$g_d(k_{sat}) = 1, \quad (22)$$

with $g_d(k) \equiv f_d(0, k)$.

In the last two columns of Table I, we show the quark saturation densities in SNM and in PNM. In the NR limit, we find that, when $r_p = 0.8$ fm, $\rho_{sat}/\rho_0 \simeq 1.27$ in SNM. Here, we take $\rho_0 = 0.15$ fm⁻³. In contrast, when $m = 300$ MeV and $r_p = 0.8$ fm, the present relativistic calculation predicts $\rho_{sat}/\rho_0 \simeq 1.63$, which is larger than in the NR result. This discrepancy is caused by the lower component of the relativistic wavefunction, which enhances the higher momentum part in the quark momentum distribution. Furthermore, the quark saturation density in SNM is larger than that in PNM by about 30%. Such tendency is seen in the IdylliQ model as well, although the difference in the IdylliQ model is tiny. In SNM, if $r_p = 1.0$ fm, normal nuclear matter might be already quarkyonic [27]. In PNM, in the cases of $r_p = 0.9$ and 1.0 fm, ρ_{sat} is lower than ρ_0 . We note that, in Ref. [28], using the transverse momentum densities for the valence and sea quarks in a nucleon, ρ_{sat}/ρ_0 is estimated to be about 1.13.

The quark saturation density strongly depends on the radius of the nucleon. However, the dependence on the quark mass is weak, i.e. fixing r_p , the difference between ρ_{sat} in the case 1 and that in case 3 is less than 10%. Hence, hereafter, we consider the case 2, i.e. $m = 300$ MeV, only.

4. Postsaturation region

Above the quark saturation density, the low momentum levels of quarks are fully occupied, where the quarks behave like Fermi gas but still feel the confinement force, i.e. *soft deconfinement*. Such region is denoted by $0 \leq q \leq q_b$, and we posit $f_{Q(d)}^{<q_b}(q) = \theta(q_b - q)$ for SNM (PNM). Correspondingly, because the dual nucleon momentum distribution is strongly suppressed by the quark Pauli blocking, it is given by $f_{N(n)}^{<k_b}(k) = 1 \left(\frac{3}{2}\right) \times \frac{1}{N_c^3} \theta(k_b - k)$, which is the under-occupied bulk part with $k_b = N_c q_b$.

On the other hand, for the higher momentum states of quarks, i.e. $q > q_b$, the levels are not fully occupied, and thus the quark momentum distribution is expected to be expressed by $\theta(q - q_b) f_{Q(d)}^{>q_b}(q)$, where $f_{Q(d)}^{>q_b}(q_b) = 1$ and $f_{Q(d)}^{>q_b}(q)$ is a gaussian function which decreases from unity as q increases. In this region, because the Pauli blocking does not work, the nucleon distribution is not suppressed and the nucleons should form the ordinary shell structure, i.e. $f_{N(n)}^{>k_b}(k) = \theta(k_s - k) \theta(k - k_b)$, where k_s is the upper bound given by $\rho_{N(n)}$. Thus, through the sum rule with $f_{N(n)}^{>k_b}(k)$, $f_{Q(d)}^{>q_b}(q)$ may be approximately given by the *shifted* distribution, $f_{Q(d)}(q - q_b, k_{sat})$, as discussed in Ref. [64]. In the nucleon matter viewpoint, it is thus expected that the nucleon momentum distributions for SNM and PNM can be expressed as

$$f_N(k) = \frac{1}{N_c^3} \theta(k_b - k) + \theta(k_s - k) \theta(k - k_b) \quad \text{for SNM}, \quad (23)$$

$$f_n(k) = \frac{3}{2N_c^3} \theta(k_b - k) + \theta(k_s - k) \theta(k - k_b) \quad \text{for PNM}. \quad (24)$$

Now, the problem is how we should determine the momenta at the boundary, k_b , and at the upper bound, k_s . Substituting the momentum distributions, Eqs. (23) and (24), into the sum rules, Eqs. (17) and (20), respectively, we can calculate the quark momentum distributions in the postsaturation region. Then, at $q = 0$, their values should be *unity*:

$$g_Q(k_s) - \beta g_Q(k_b) = 1 \quad \text{for SNM}, \quad (25)$$

$$g_d(k_s) - \beta' g_d(k_b) = 1 \quad \text{for PNM}, \quad (26)$$

with $\beta = 1 - 1/N_c^3$ and $\beta' = 1 - 3/(2N_c^3)$. Note that, when $k_s = k_{sat}$, k_b vanishes. The boundary conditions, Eqs. (25) and (26), are the *necessary* condition, and are identical to the condition that sets the relation between k_b and k_s in the IdylliQ model [24]. Thus, in this paper, together with Eqs. (14) and (15), we shall take these boundary conditions to determine k_b and k_s .

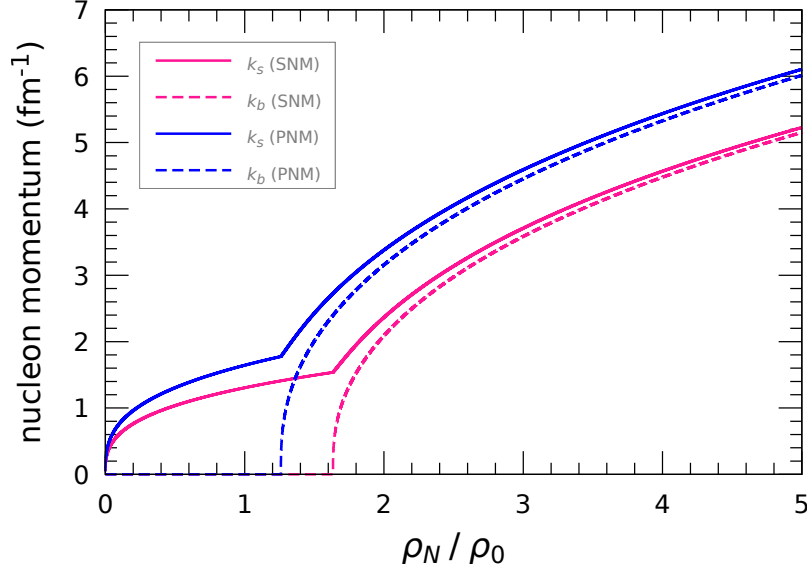


FIG. 1. Density dependence of k_s and k_b in the case of $r_p = 0.8$ fm.

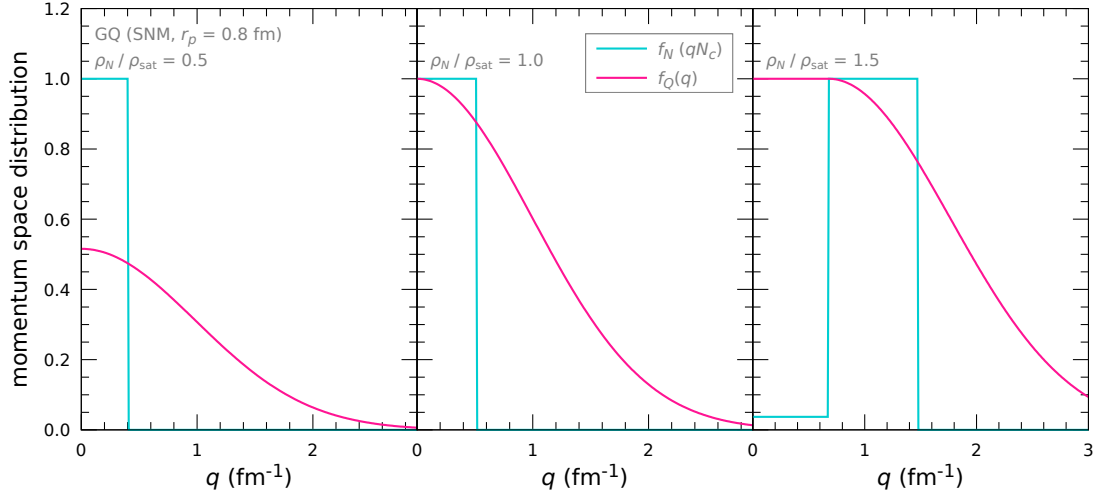


FIG. 2. Quark and nucleon momentum distributions in symmetric nuclear matter. We take $r_p = 0.8$ fm.

In Fig. 1, we show the density dependence of k_b and k_s in SNM or in PNM. The rapid rise of the momenta, k_b and k_s , occurs beyond ρ_{sat} , which leads to singular behavior of thermodynamical quantities. Furthermore, in Fig. 2, we illustrate the quark and nucleon momentum distributions, $f_Q(q)$ and $f_N(k)$, in symmetric nuclear matter. The quark distri-

bution in the postsaturation region (right panel) is estimated by following the procedure in Ref. [64].

B. Initial results

Using the GQ model, we evaluate the energy density, chemical potential, pressure and sound velocity in the viewpoint of nucleon matter.

1. Symmetric nuclear matter

First, the nuclear density, Eq. (14), reads

$$\rho_N^{below} = \frac{2}{3\pi^2} k_s^3 \quad (k_s = k_F), \quad (27)$$

$$\rho_N^{above} = \frac{2}{3\pi^2} (k_s^3 - \beta k_b^3), \quad (28)$$

where the superscripts (below, above) indicate ($\rho_N < \rho_{sat}$, $\rho_N > \rho_{sat}$), respectively. Because, in the limit $\rho_N \rightarrow \rho_{sat}$, k_b approaches zero, the density is continuous at ρ_{sat} . The derivative of the density with respect to k_s is then given by

$$\frac{\partial \rho_N^{below}}{\partial k_s} = \frac{2}{\pi^2} k_s^2, \quad (29)$$

$$\frac{\partial \rho_N^{above}}{\partial k_s} = \frac{2}{\pi^2} k_s^2 \left[1 - \beta \frac{k_b^2}{k_s^2} \frac{\partial k_b}{\partial k_s} \right] = \frac{2}{\pi^2} k_s^2 \left[1 - \frac{k_b^2}{k_s^2} \frac{\phi(k_s)}{\phi(k_b)} \right]. \quad (30)$$

Here, the derivative of k_b with respect to k_s is calculated by the boundary condition, Eq. (25), as

$$\frac{\partial k_b}{\partial k_s} = \frac{1}{\beta} \frac{\phi(k_s)}{\phi(k_b)} = \frac{1}{\beta} \frac{r_1(k_s) \bar{k}_s^2}{r_1(k_b) \bar{k}_b^2} e^{-\bar{k}_s^2 + \bar{k}_b^2}, \quad (31)$$

where we define

$$\phi(k) \equiv \frac{\partial}{\partial \bar{k}} g_Q(k) = \frac{N_c^3}{\sqrt{\pi}} [4r_1(k) \bar{k}^2] e^{-\bar{k}^2}, \quad (32)$$

with

$$r_n(k) = 1 - \frac{(2n+1) - 2\bar{k}^2}{2\bar{\lambda}^2 + 3}. \quad (33)$$

Note that $g_Q(k)$ and $\phi(k)$ are dimensionless.

In Eq. (30), the second term in the right-hand side has the factor k_b^2 coming from the Jacobian, but it is completely canceled by the factor k_b^{-2} in Eq. (31). This is an outstanding

characteristic in the case of gaussian quark wavefunction. Thus, unfortunately, for chemical potential, pressure or sound velocity, the continuity at ρ_{sat} does *not* hold.

We next calculate the energy density, ϵ_N . We find

$$\epsilon_N^{below} = \frac{2}{\pi^2} \int_0^{k_s} dk k^2 E_N(k) = \frac{2}{\pi^2} I(M_N, k_s), \quad (34)$$

$$\epsilon_N^{above} = \frac{2}{\pi^2} \left(\int_0^{k_s} - \beta \int_0^{k_b} \right) dk k^2 E_N(k) = \frac{2}{\pi^2} [I(M_N, k_s) - \beta I(M_N, k_b)], \quad (35)$$

with $E_N(k) = \sqrt{M_N^2 + k^2}$ and

$$\begin{aligned} I(M, x) &= \int_0^x dt t^2 \sqrt{M^2 + t^2} \\ &= \frac{1}{8} \left[x(M^2 + 2x^2) \sqrt{M^2 + x^2} + M^4 \log \left(\frac{M}{x + \sqrt{M^2 + x^2}} \right) \right]. \end{aligned} \quad (36)$$

Therefore, the energy density is continuous at ρ_{sat} . However, the first derivatives are given by

$$\frac{\partial \epsilon_N^{below}}{\partial k_s} = \frac{2}{\pi^2} k_s^2 E_N(k_s), \quad (37)$$

$$\frac{\partial \epsilon_N^{above}}{\partial k_s} = \frac{2}{\pi^2} k_s^2 E_N(k_s) \left[1 - \beta \frac{k_b^2 E_N(k_b)}{k_s^2 E_N(k_s)} \frac{\partial k_b}{\partial k_s} \right] = \frac{2}{\pi^2} k_s^2 E_N(k_s) \left[1 - \frac{k_b^2 E_N(k_b)}{k_s^2 E_N(k_s)} \frac{\phi(k_s)}{\phi(k_b)} \right]. \quad (38)$$

So, the derivative has a gap at ρ_{sat} .

The chemical potential, $\mu_N = \partial \epsilon_N / \partial \rho_N$, is similarly evaluated as

$$\mu_N^{below} = E_N(k_s), \quad \frac{\partial \mu_N^{below}}{\partial k_s} = \frac{k_s}{E_N(k_s)}, \quad (39)$$

$$\mu_N^{above} = E_N(k_s) \frac{1 - \frac{k_b^2 E_N(k_b)}{k_s^2 E_N(k_s)} \frac{\phi(k_s)}{\phi(k_b)}}{1 - \frac{k_b^2}{k_s^2} \frac{\phi(k_s)}{\phi(k_b)}}. \quad (40)$$

The ratio of μ_N^{above} to μ_N^{below} gives the gap of chemical potential at ρ_{sat} , and it is

$$\frac{\mu_N^{above}}{\mu_N^{below}} = \frac{1 - \left[\frac{r_1(k_s) E_N(k_b)}{r_1(k_b) E_N(k_s)} \right] e^{-\bar{k}_s^2 + \bar{k}_b^2}}{1 - \left[\frac{r_1(k_s)}{r_1(k_b)} \right] e^{-\bar{k}_s^2 + \bar{k}_b^2}} > 1. \quad (41)$$

We can calculate pressure, P , by using ρ_N , ϵ_N , and μ_N

$$P = \mu_N \rho_N - \epsilon_N. \quad (42)$$

Therefore, pressure has a gap at ρ_{sat} as well.

Finally, the (squared) sound velocity, v_s^2 , is estimated by

$$v_s^2 = \frac{\rho_N}{\mu_N} \left(\frac{\partial \mu_N}{\partial \rho_N} \right). \quad (43)$$

Below ρ_{sat} , the sound velocity reads

$$v_s^{2\,below} = \frac{k_s^2}{3E_N(k_s)^2}. \quad (44)$$

To calculate $v_s^{2\,above}$, we need the second derivative, $\partial^2 k_b / \partial k_s^2$, which is again derived from the boundary condition, Eq. (25). We then obtain

$$\frac{\partial^2 k_b}{\partial k_s^2} = \frac{1}{\beta} \left[\frac{\phi'(k_s)}{\phi(k_b)} - \beta \left(\frac{\partial k_b}{\partial k_s} \right)^2 \frac{\phi'(k_b)}{\phi(k_b)} \right] \xrightarrow{k_b \rightarrow 0} k_b^{-5}, \quad (45)$$

with

$$\phi'(k) = \frac{N_c^3}{\sqrt{\pi}} 8\bar{k} [r_1(k) - r_2(k)\bar{k}^2] e^{-\bar{k}^2}. \quad (46)$$

Thus, the sound velocity reads

$$v_s^{2\,above} = \frac{\rho_N^{above}}{\mu_N^{above}} \left(\frac{\partial \mu_N^{above}}{\partial k_s} \right) / \left(\frac{\partial \rho_N^{above}}{\partial k_s} \right), \quad (47)$$

where

$$\frac{\partial \mu_N^{above}}{\partial k_s} = \mu_N^{above} \times \left(\frac{A'}{A} - \frac{B'}{B} \right), \quad (48)$$

with

$$A = k_s^2 E_N(k_s) - \beta k_b^2 E_N(k_b) \frac{\partial k_b}{\partial k_s}, \quad (49)$$

$$B = k_s^2 - \beta k_b^2 \frac{\partial k_b}{\partial k_s}, \quad (50)$$

$$A' = 2k_s E_N(k_s) + \frac{k_s^3}{E_N(k_s)} - \beta \left[k_b^2 E_N(k_b) \frac{\partial^2 k_b}{\partial k_s^2} + \left(2k_b E_N(k_b) + \frac{k_b^3}{E_N(k_b)} \right) \left(\frac{\partial k_b}{\partial k_s} \right)^2 \right], \quad (51)$$

$$B' = 2k_s - \beta \left[k_b^2 \frac{\partial^2 k_b}{\partial k_s^2} + 2k_b \left(\frac{\partial k_b}{\partial k_s} \right)^2 \right]. \quad (52)$$

In Fig. 3, we show ϵ_N , μ_N , P and v_s^2 in the case of $r_p = 0.6$ or 0.8 fm. At ρ_{sat} , the energy density is continuous, but is not smooth, while there is a large gap in the chemical potential or pressure, which may not be permitted in thermodynamics. The sound velocity diverges at ρ_{sat} , as seen in the IdylliQ model.

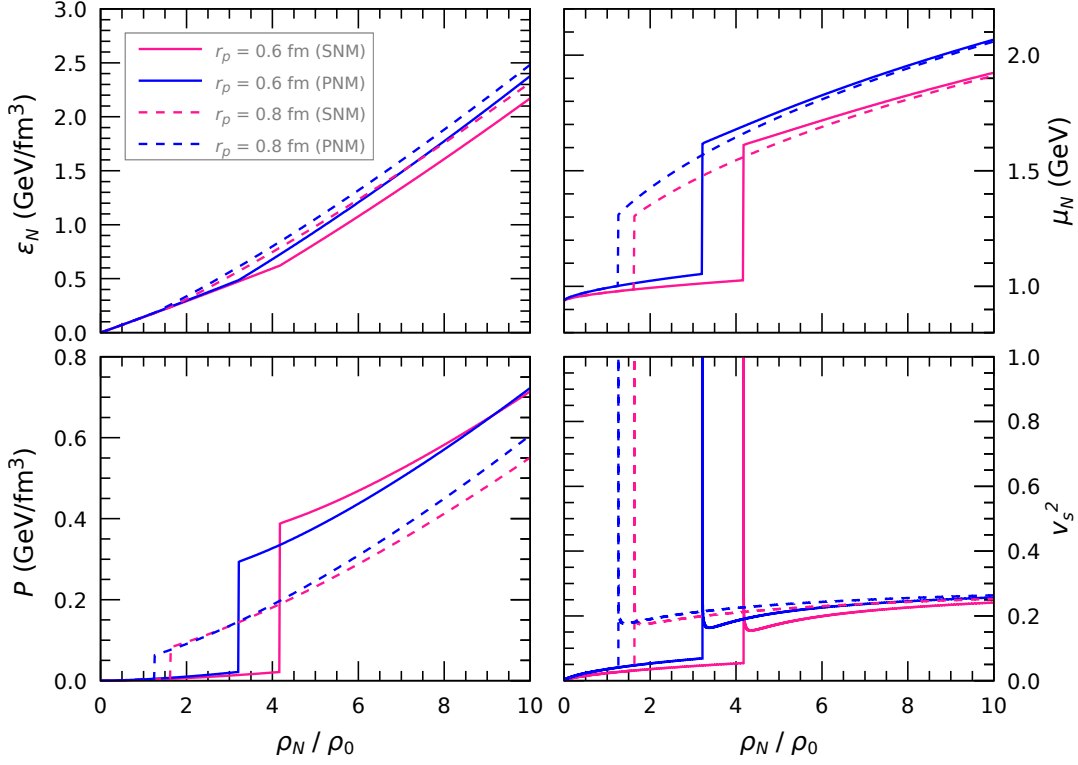


FIG. 3. Energy density, chemical potential, pressure or sound velocity as a function of ρ_N .

2. Pure neutron matter

For PNM, the neutron density reads

$$\rho_n^{below} = \frac{1}{3\pi^2} k_s^3 \quad (k_s = k_F), \quad (53)$$

$$\rho_n^{above} = \frac{1}{3\pi^2} (k_s^3 - \beta' k_b^3), \quad (54)$$

and the energy density is

$$\epsilon_n^{below} = \frac{1}{\pi^2} \int_0^{k_s} dk k^2 E_n(k) = \frac{1}{\pi^2} I(M_N, k_s), \quad (55)$$

$$\epsilon_n^{above} = \frac{1}{\pi^2} \left(\int_0^{k_s} -\beta' \int_0^{k_b} \right) dk k^2 E_n(k) = \frac{1}{\pi^2} [I(M_N, k_s) - \beta' I(M_N, k_b)], \quad (56)$$

with $E_n(k) = \sqrt{M_N^2 + k^2}$. Then, replacing N_c^3 with $\frac{2}{3} N_c^3$, we can calculate μ_n , P , and v_s^2 as in case of SNM. Fig. 3 depicts ϵ_n , μ_n , P , and v_s^2 in PNM as well.

C. Gaussian quarkyonic model with minimal corrections

As seen in Section II B, we have encountered the singular behavior of physical quantities in the naïve GQ model. We thus need to somehow remedy such behavior. Because the cause of gap and divergence at the quark saturation density comes from $\phi(k_b)$ in Eq. (31), which is related to $\partial g_{Q(d)}(k_b)/\partial k_b$, the minimal correction to cure this problem can be provided with a smearing of the sharp Fermi surface, $\theta(k_b - k)$, in the nucleon distributions, Eqs. (23) and (24). Originally, such a smearing should be evaluated by the quark and gluon exchanges among nucleons, but it is extremely difficult to handle them in a multi-baryon system. Instead, for example, we could apply Sommerfeld expansion to blur the Fermi surface phenomenologically – for the detail, see Appendix A.

In this paper, we however take another, more practical prescription to remove the singular behavior in the initial model. Here, we want to modify k_b^2 in the denominator of Eq. (31) so that the power of k_b is weaker. In the method of Sommerfeld expansion, the power of k_b is eventually weaken (see Appendix A). To do so, we shall introduce an infrared regulator to the boundary conditions, Eqs. (25) and (26). Then, we take the simplest choice

$$\alpha_\nu(k_b) = 1 + \left(\frac{w}{k_b}\right)^\nu \rightarrow \infty (1) \text{ as } k_b \rightarrow 0 (\infty), \quad (57)$$

with w a width parameter and ν a positive, real number. The boundary conditions are thus redefined by

$$g_Q(k_s) - \beta \alpha_\nu(k_b) g_Q(k_b) = 1 \quad \text{for SNM}, \quad (58)$$

$$g_d(k_s) - \beta' \alpha_\nu(k_b) g_d(k_b) = 1 \quad \text{for PNM}. \quad (59)$$

Note that, when $w = 0$, $\alpha_\nu = 1$ (without the regulator). Because $g_{Q(d)}(k_b)$ behaves like $\mathcal{O}(k_b^3)$ when $k_b \rightarrow 0$, the parameter, ν , should be taken as $0 < \nu < 3$. Furthermore, we find

$$\alpha'_\nu(k_b) \equiv \frac{d}{dk_b} \alpha_\nu(k_b) = -\frac{\nu}{\bar{w}} \left(\frac{w}{k_b}\right)^{\nu+1}, \quad (60)$$

$$\alpha''_\nu(k_b) \equiv \frac{d^2}{dk_b^2} \alpha_\nu(k_b) = \frac{\nu(\nu+1)}{\bar{w}^2} \left(\frac{w}{k_b}\right)^{\nu+2}, \quad (61)$$

where $\bar{w}(\equiv aw/N_c)$, α_ν , α'_ν , and α''_ν are all dimensionless. Fig. 4 depicts the momenta, k_b and k_s , calculated with the modified boundary condition, Eqs. (58) and (59). We notice that the momenta increase gradually beyond the quark saturation density, compared with the result without the regulator.

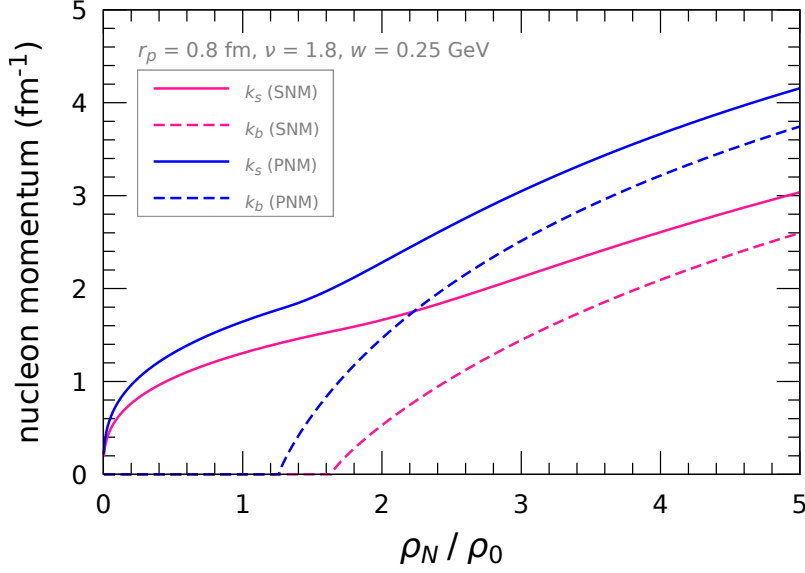


FIG. 4. Density dependence of k_s and k_b in the case of $r_p = 0.8$ fm. We take $\nu = 1.8$ and $w = 0.25$ GeV.

In the case of SNM, using the modified boundary condition, the first derivative, $\partial k_b / \partial k_s$, reads

$$\frac{\partial \bar{k}_b}{\partial \bar{k}_s} = \frac{\partial k_b}{\partial k_s} = \frac{\phi(k_s)}{\beta[\alpha'_\nu(k_b)g_Q(k_b) + \alpha_\nu(k_b)\phi(k_b)]} \xrightarrow{k_b \rightarrow 0} k_b^{\nu-2}, \quad (62)$$

which ensures that the physical quantities (except v_s^2) are continuous at the quark saturation density. Similarly, using the modified boundary condition again, the second derivative reads

$$\frac{\partial^2 \bar{k}_b}{\partial \bar{k}_s^2} = \left(\frac{N_c}{a}\right) \frac{\partial^2 k_b}{\partial k_s^2} = \frac{\phi'(k_s) - \beta \left(\frac{\partial \bar{k}_b}{\partial \bar{k}_s}\right)^2 X(k_b)}{\beta[\alpha'_\nu(k_b)g_Q(k_b) + \alpha_\nu(k_b)\phi(k_b)]} \xrightarrow{k_b \rightarrow 0} k_b^{2\nu-5}, \quad (63)$$

with

$$X(k_b) \equiv \frac{\partial^2}{\partial \bar{k}_b^2} \alpha_\nu(k_b)g_Q(k_b) = \alpha''_\nu(k_b)g_Q(k_b) + 2\alpha'_\nu(k_b)\phi(k_b) + \alpha_\nu(k_b)\phi'(k_b). \quad (64)$$

Therefore, to make the sound velocity continuous and make μ_N and P smooth at ρ_{sat} , the parameter, ν , is further restricted to be $\frac{3}{2} < \nu < 3$ (see Eqs. (51) and (52)). For PNM, it is necessary to replace β with β' .

Now, we can calculate ϵ_N , μ_N , P , and v_s^2 , as in Section II B, replacing $\partial k_b / \partial k_s$ and $\partial^2 k_b / \partial k_s^2$ with the modified ones. In Fig. 5, we present the result in SNM or PNM. As expected, ϵ_N , μ_N , P , and v_s^2 are all continuous, and ϵ_N , μ_N and P are smooth at ρ_{sat} .

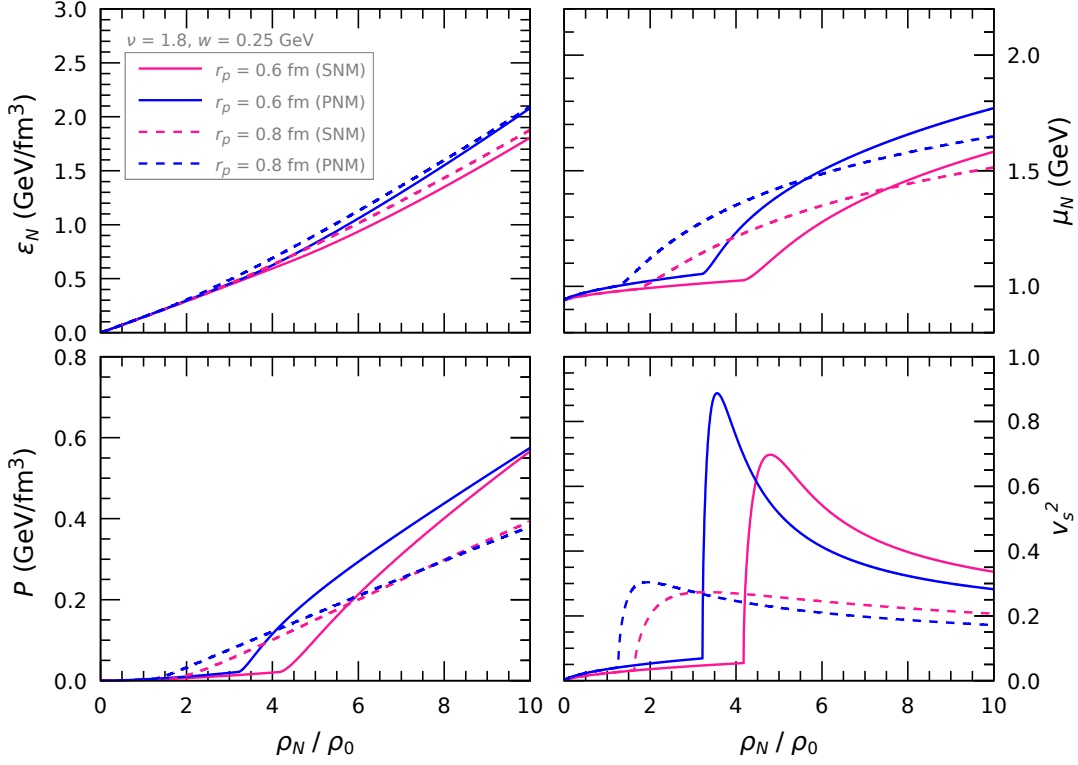


FIG. 5. Energy density, chemical potential, pressure and sound velocity in the case of $\nu = 1.8$ and $w = 0.25$ GeV.

Furthermore, Fig. 6 and (7) respectively show the dependences of μ_N and v_s^2 on ν and w in detail. It is seen that, in the chemical potential, as the width parameter, w , is larger, μ_N beyond ρ_{sat} is more suppressed, and that the larger power, ν , tames the rapid rise at ρ_{sat} more. We can see the similar trend in v_s^2 as well. The sound velocity with $w = 0.1$ GeV does not diverge at ρ_{sat} , but overshoots the upper limit. The same occurs in the case of $r_p = 0.6$ fm and $w = 0.2$ GeV. The parameter, w , broadens the peak of the sound velocity, while ν enhances the height of the peak and hinders the rapid increase of the velocity around ρ_{sat} .

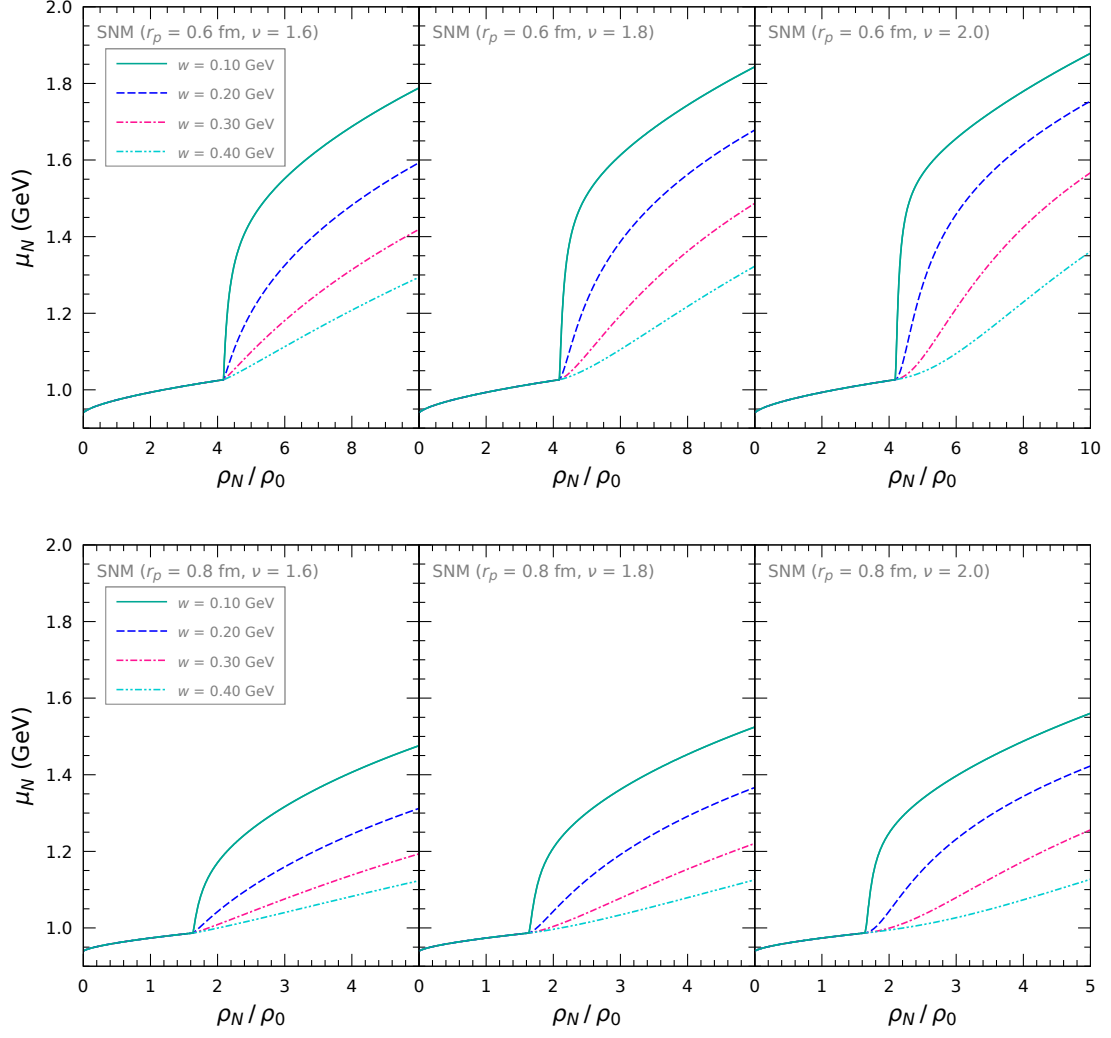


FIG. 6. Dependence of chemical potential on ν and w in SNM. The upper (lower) panel is for $r_p = 0.6$ (0.8) fm.

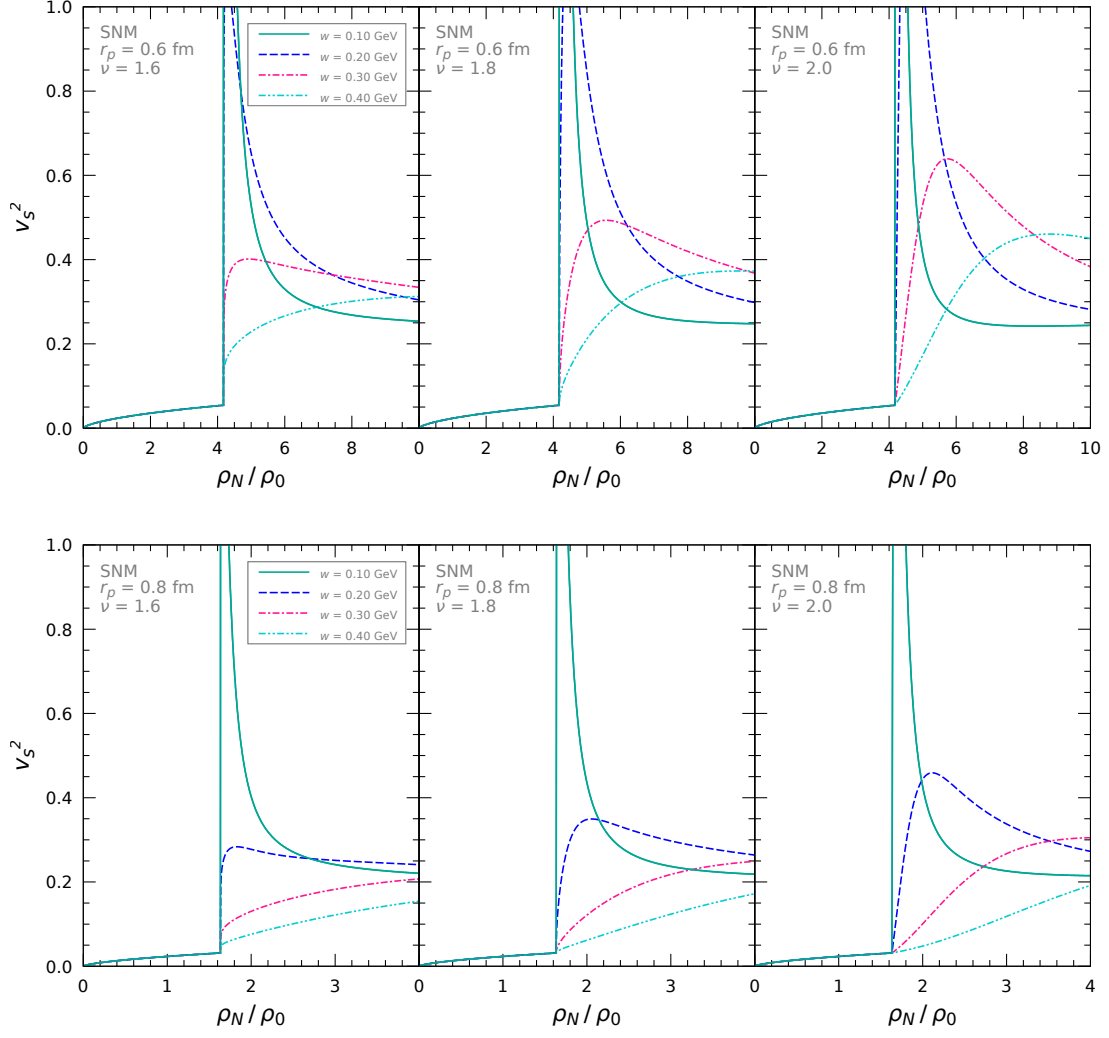


FIG. 7. Dependence of sound velocity on ν and w in SNM. The upper (lower) panel is for $r_p = 0.6$ (0.8) fm.

III. QUARKYONIC QUARK-MESON COUPLING MODEL

We here build a new, quark-based nuclear model, in which we incorporate the GQ model into the QMC model. The two models are combined each other through the gaussian quark wavefunction, Eq. (5). We will call it the quarkyonic quark-meson coupling (QQMC) model.

A. Brief review of the QMC model

In this section, we briefly review the quark-meson coupling (QMC) model with the gaussian quark wavefunction.

We here consider the mean fields of σ , ω , and ρ mesons, which interact with the confined quarks, in uniformly distributed, asymmetric nuclear matter. Let the mean-field values for the σ , ω (the time component) and ρ (the time component in the 3rd direction of isospin) fields be $\bar{\sigma}$, $\bar{\omega}$ and $\bar{\rho}$, respectively.

Under the relativistic HO potential, Eq. (4), the Dirac equation for the quark field ψ_j ($j = u$ or d) is given by [58]

$$\left[i\gamma \cdot \partial - (m - V_s) - \gamma_0 V_0 - \frac{c}{2} (1 + \gamma_0) r^2 \right] \psi_j(\mathbf{r}, t) = 0, \quad (65)$$

where $V_s = g_\sigma^q \bar{\sigma}$ and $V_0 = g_\omega^q \bar{\omega} + \tau_{3j} g_\rho^q \bar{\rho}$ [$\tau_{3j} = \pm 1$ for $\binom{u}{d}$ quark] with the quark-meson coupling constants, g_σ^q , g_ω^q and g_ρ^q . Note that the isoscalar σ meson couples to the u and d quarks equally. We respectively define the effective quark mass and the effective single-particle quark energy as $m^* \equiv m - V_s = m - g_\sigma^q \bar{\sigma}$ and $\epsilon^* \equiv \epsilon_j - V_0 = \epsilon_j - g_\omega^q \bar{\omega} \mp g_\rho^q \bar{\rho}$ for $\binom{u}{d}$ quark, where ϵ_j is the eigenenergy of Eq. (65). The static, lowest-state wavefunction in matter is presented by

$$\psi_j(\mathbf{r}, t) = \exp[-i\epsilon_j t] \psi_Q(\mathbf{r}). \quad (66)$$

The wavefunction $\psi_Q(\mathbf{r})$ is then given by Eqs. (5) and (6), in which ϵ , m , λ and a are, respectively, replaced with ϵ^* , m^* , λ^* and a^* , and the effective energy ϵ^* is determined by $\sqrt{\epsilon^* + m^*}(\epsilon^* - m^*) = 3\sqrt{c}$ (see Eq. (7)). We assume that the strength parameter, c , of the confinement potential does not change in matter.

The zeroth-order energy of the nucleon in matter is thus given by $E_N^{0*} = 3\epsilon^*$, and we have the effective nucleon mass in matter ($M_N^* = M_p^* = M_n^*$)

$$M_N^* = E_B^{0*} + E_N^{spin} - E_N^{c.m.*}. \quad (67)$$

Here, we assume that the spin correlation E_N^{spin} does not change in matter, and the c.m. correction $E_N^{c.m.*}$ is given by Eq. (8) with ϵ^* and m^* , instead of ϵ and m .

For describing asymmetric nuclear matter, we now start from the following Lagrangian density in mean-field approximation [37]

$$\begin{aligned} \mathcal{L} = & \bar{\psi}_N [i\gamma \cdot \partial - M_N^*(\bar{\sigma}) - g_\omega \gamma_0 \bar{\omega} - g_\rho \gamma_0 \tau_3 \bar{\rho}] \psi_N \\ & - \frac{m_\sigma^2}{2} \bar{\sigma}^2 + \frac{m_\omega^2}{2} \bar{\omega}^2 + \frac{m_\rho^2}{2} \bar{\rho}^2 - \frac{g_2}{3} \bar{\sigma}^3 \end{aligned} \quad (68)$$

with ψ_N the nucleon field, and τ_3 the 3rd component of Pauli matrix. The nucleon-meson coupling constants, g_σ , g_ω , and g_ρ , are respectively related to the quark-meson coupling constants as $g_\sigma = 3g_\sigma^q$, $g_\omega = 3g_\omega^q$, and $g_\rho = g_\rho^q$. The meson masses are taken to be $m_\sigma = 550$ MeV, $m_\omega = 783$ MeV, and $m_\rho = 770$ MeV. We add the last term to the Lagrangian, which is the nonlinear, self-coupling term of σ meson, in order to reproduce the properties of nuclear matter as discussed later. Here, we do not include the nonlinear term $\frac{1}{4}g_3\sigma^4$, because it plays similar roles as $\frac{1}{3}g_2\sigma^3$.

The total energy per nucleon of asymmetric nuclear matter is then obtained by

$$\begin{aligned} \epsilon_{tot}/\rho_N = & \epsilon_N^*/\rho_N + g_\omega \bar{\omega} + g_\rho \left(\frac{\rho_3}{\rho_N} \right) \bar{\rho} \\ & + \frac{1}{2\rho_N} (m_\sigma^2 \bar{\sigma}^2 - m_\omega^2 \bar{\omega}^2 - m_\rho^2 \bar{\rho}^2) + \frac{1}{3\rho_N} g_2 \bar{\sigma}^3, \end{aligned} \quad (69)$$

where

$$\epsilon_N^* = \frac{1}{\pi^2} \int dk k^2 E_N^*(k) [f_p(k) + f_n(k)], \quad (70)$$

with $E_N^*(k) = \sqrt{M_N^{*2} + k^2}$. Note that $f_{i=p,n}(k) = \theta(k_{F_i} - k)$ with k_{F_i} the Fermi momentum for protons or neutrons, which is related to the density of protons (neutrons), $\rho_{p(n)}$, through $\rho_{p(n)} = k_{F_{p(n)}}^3/(3\pi^2)$. The total nucleon density is given by $\rho_N = \rho_p + \rho_n$, and the difference in proton and neutron densities is defined by $\rho_3 \equiv \rho_p - \rho_n$. The binding energy per nucleon, ϵ_b , is given by $\epsilon_b(\rho_N) = \epsilon_{tot}/\rho_N - M_N$.

The mean-field values for the mesons satisfy [58]

$$(m_\sigma^2 + g_2 \bar{\sigma}) \bar{\sigma} = - \left(\frac{\partial M_N^*}{\partial \bar{\sigma}} \right) (\rho_p^s + \rho_n^s) \equiv g_\sigma G_\sigma(\bar{\sigma}) (\rho_p^s + \rho_n^s), \quad (71)$$

$$m_\omega^2 \bar{\omega} = g_\omega \rho_N, \quad (72)$$

$$m_\rho^2 \bar{\rho} = g_\rho \rho_3, \quad (73)$$

where Eq. (71) is the gap equation for the nucleon mass in matter. Here, $\rho_{i=p(n)}^s$ is the scalar density of protons (neutrons) in matter

$$\rho_i^s = \frac{1}{\pi^2} \int dk k^2 \frac{M_N^*}{\sqrt{M_N^{*2} + k^2}} f_i(k) = \frac{M_N^*}{\pi^2} J(M_N^*, k_{F_i}). \quad (74)$$

with

$$\begin{aligned} J(M, x) &= \int_0^x dt \frac{t^2}{\sqrt{M^2 + t^2}} \\ &= \frac{1}{2} \left[x \sqrt{M^2 + x^2} + M^2 \log \left(\frac{M}{x + \sqrt{M^2 + x^2}} \right) \right]. \end{aligned} \quad (75)$$

Furthermore, $G_\sigma(\bar{\sigma})$ is the quark scalar density in the nucleon, i.e. *the isoscalar, Lorentz scalar polarizability* [58]

$$G_\sigma(\bar{\sigma}) \equiv S^*(\bar{\sigma}) - \frac{1}{3} \frac{\partial}{\partial m^*} E_N^{c.m.*}, \quad (76)$$

where

$$S^*(\bar{\sigma}) = \frac{\partial \epsilon^*}{\partial m^*} = \frac{\epsilon^* + 3m^*}{3\epsilon^* + m^*}, \quad (77)$$

$$\begin{aligned} \frac{1}{3} \frac{\partial}{\partial m^*} E_N^{c.m.*} &= \frac{1}{27} \left[\frac{2(\epsilon^* S^* - m^*)(77\epsilon^* + 31m^*)}{(3\epsilon^* + m^*)^2} + \frac{(\epsilon^{*2} - m^{*2})(77S^* + 31)}{(3\epsilon^* + m^*)^2} \right. \\ &\quad \left. - 2 \frac{(\epsilon^{*2} - m^{*2})(77\epsilon^* + 31m^*)(3S^* + 1)}{(3\epsilon^* + m^*)^3} \right]. \end{aligned} \quad (78)$$

Now, we have four parameters, g_σ , g_ω , g_ρ and g_2 . The coupling constants, g_σ and g_ω , are determined so as to fit the binding energy, $\epsilon_b(\rho_0) = -16$ MeV, at the nuclear saturation density in equilibrium, symmetric nuclear matter. We fit the ρ -nucleon coupling constant so as to reproduce the bulk symmetry energy of symmetric nuclear matter, $E_{sym}(\rho_0) = 32.0$ MeV. Finally, the nonlinear coupling constant, g_2 , is used to fit the nuclear incompressibility, $K_0 = 240$ MeV.

The coupling constants and the properties of nucleons and nuclear matter in the case 2 are, respectively, listed in Tables II and III. At ρ_0 , the root-mean-square charge radius of proton, r_p^* , increases by about 5% compared with the radius in vacuum, r_p . This swelling is consistent with the experiments (see Ref. [42]). We also calculate the slope and the curvature parameters of nuclear symmetry energy, L and K_{sym} , which are related to astrophysical multi-messenger observations of neutron stars [65, 66].

The binding energy per nucleon and pressure are showed in Fig. 8. Fig. 9 illustrates the mean-field value for the σ meson in SNM. The increase of the scalar field becomes slower at

TABLE II. Coupling constants in the case 2. For the detail, see the text.

| r_p (fm) | g_σ | g_ω | g_ρ | g_2 (fm $^{-1}$) |
|------------|------------|------------|----------|---------------------|
| 0.6 | 11.00 | 7.47 | 4.36 | 22.78 |
| 0.7 | 10.49 | 7.56 | 4.36 | 23.81 |
| 0.8 | 10.11 | 7.65 | 4.35 | 24.65 |
| 0.9 | 9.83 | 7.74 | 4.35 | 25.32 |
| 1.0 | 9.61 | 7.81 | 4.34 | 25.84 |

 TABLE III. Properties of in-medium nucleons and symmetric nuclear matter at the nuclear saturation density, ρ_0 , in the case 2. Here, L and K_{sym} are, respectively, the slope and the curvature parameters of nuclear symmetry energy. The quark saturation densities in matter are listed in the last two columns (see Section III B).

| r_p | r_p^* | m^* | ϵ^* | M_N^* | E_N^{0*} | $E_N^{c.m.*}$ | L | K_{sym} | ρ_{sat}^*/ρ_0 | |
|-------|---------|-------|--------------|---------|------------|---------------|------|-----------|-----------------------|-------|
| (fm) | | | | | (MeV) | | | | SNM | PNM |
| 0.6 | 0.627 | 223.5 | 620.4 | 776.5 | 1861.2 | 468.4 | 86.4 | -18.1 | 3.594 | 2.826 |
| 0.7 | 0.733 | 226.7 | 541.6 | 773.8 | 1624.9 | 382.2 | 86.5 | -17.5 | 2.212 | 1.740 |
| 0.8 | 0.840 | 228.9 | 484.7 | 771.1 | 1454.1 | 318.0 | 86.6 | -16.9 | 1.459 | 1.146 |
| 0.9 | 0.946 | 230.5 | 442.1 | 768.6 | 1326.4 | 268.7 | 86.7 | -16.3 | 1.012 | 0.794 |
| 1.0 | 1.053 | 231.7 | 409.4 | 766.1 | 1228.3 | 230.0 | 86.8 | -15.7 | 0.730 | 0.572 |

high density, compared with that at low density, which generates the nuclear saturation with a moderate value of incompressibility, K_0 [35]. In Fig. 10, we present the density dependence of the effective quark mass or that of the effective nucleon mass in SNM. Fig. 11 depicts the scalar polarizability, G_σ . In matter, the quark mass is lighter, i.e. *more relativistic*, than the mass in vacuum. Therefore, the lower component in the quark wavefunction is enhanced, and thus the quark scalar density in a nucleon in matter is more reduced, i.e. $G_\sigma(0) > G_\sigma(\bar{\sigma})$, which softens the incompressibility, K_0 .

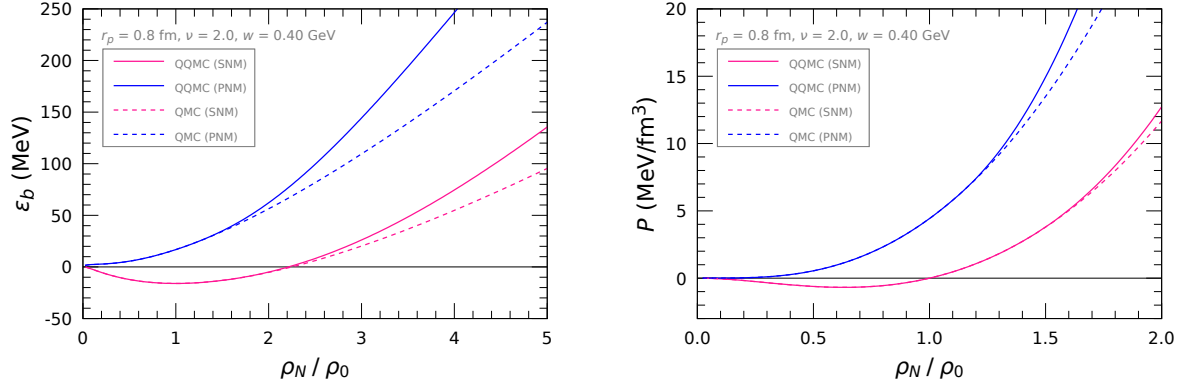


FIG. 8. Binding energy per nucleon, ϵ_b , and pressure, P , in the case of $r_p = 0.8$ fm. The dashed (solid) curves are for the QMC (QQMC) model.

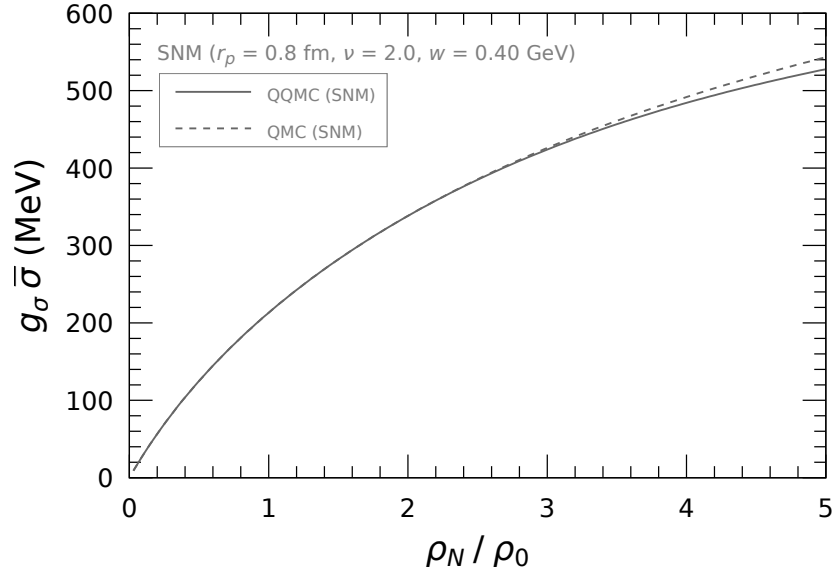


FIG. 9. Density dependence of the sigma field, $g_\sigma \bar{\sigma}$, in the case of $r_p = 0.8$ fm. The dashed (solid) curves are for the QMC (QQMC) model.

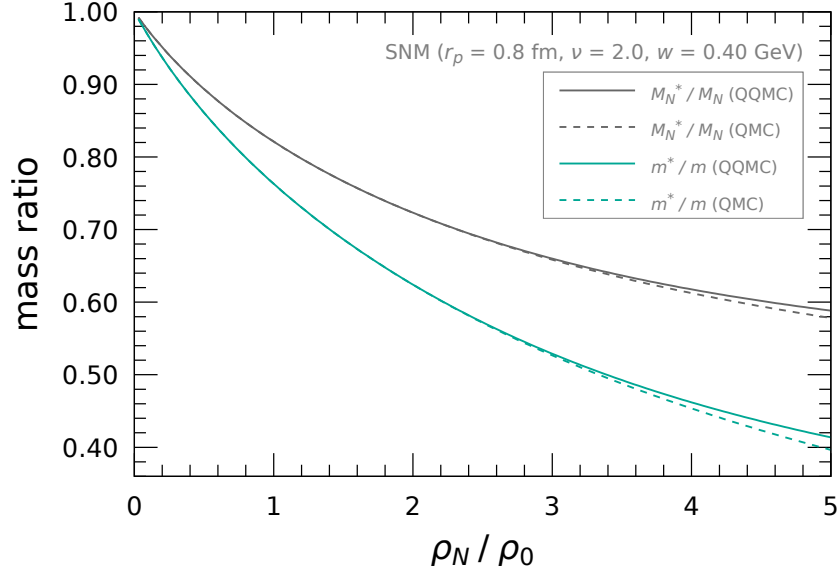


FIG. 10. Density dependence of mass ratio, M_N^*/M_N or m^*/m , in the case of $r_p = 0.8$ fm. The dashed (solid) curves are for the QMC (QQMC) model.

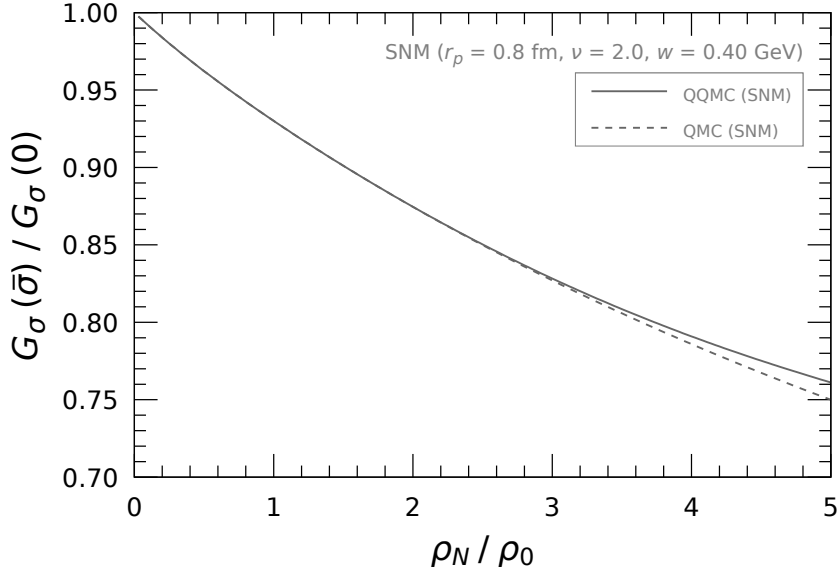


FIG. 11. Density dependence of the scalar polarizability, $G_\sigma(\bar{\sigma})/G_\sigma(0)$, in the case of $r_p = 0.8$ fm. The dashed (solid) curves are for the QMC (QQMC) model.

B. Quarkyonic QMC model

In this Section, we construct the QQMC model for symmetric nuclear matter and pure neutron matter, in which the nuclear interaction is involved at the level of mean-field approximation.

First, the quark saturation density, ρ_{sat}^* , in SNM is determined by Eq. (21) with m^* , ϵ^* , and a^* , instead of m , ϵ , and a :

$$g_Q^*(k_{sat}^*) = \frac{N_c^3}{\sqrt{\pi}} \left[\sqrt{\pi} - 2\text{Er}(\bar{k}_{sat}^*) - 2\bar{k}_{sat}^* \left(1 + \frac{2\bar{k}_{sat}^{*2}}{2\bar{\lambda}^{*2} + 3} \right) e^{-\bar{k}_{sat}^{*2}} \right] = 1, \quad (79)$$

with $\bar{\lambda}^* = a^* \lambda^*$ and $\bar{k}^* = a^* k^* / N_c$ dimensionless variables. Then, we find $\rho_{sat}^* = 2k_{sat}^{*3} / (3\pi^2)$, which is smaller than ρ_{sat} in the GQ model, because the quark wavefunction in matter is more spread out than in free space, i.e. $a^* > a$. For PNM, Eq. (22) with m^* , ϵ^* , and a^* provides the quark saturation density. In the last two columns of Table III, the quark saturation density is summarized. In fact, ρ_{sat}^* is roughly 10% smaller than ρ_{sat} .

Once the quark saturation density is found, we can realize the model in the pre and postsaturation regions as in Sec. II C. In the presaturation region, i.e. $\rho_N < \rho_{sat}^*$, the matter can be well described by the QMC model itself.

In the postsaturation region, i.e. $\rho_N > \rho_{sat}^*$, we introduce the depletion phase in the nucleon momentum distribution. The boundary for the unoccupied bulk part, k_b^* , and the upper bound of the nucleon momentum, k_s^* , in SNM are evaluated by Eq. (28), in which k_b and k_s are respectively replaced with k_b^* and k_s^* , and the modified boundary condition, Eq. (58) with k_b^* and k_s^*

$$g_Q^*(k_s^*) - \beta \alpha_\nu(k_b^*) g_Q^*(k_b^*) = 1. \quad (80)$$

For PNM, Eqs. (54) and (59) with m^* , ϵ^* , and a^* generate the two momenta, k_b^* and k_s^* . Fig. 12 depicts the density dependence of k_b^* and k_s^* . In the calculation of the QQCM model, as discussed in the end of this section, we adjust the parameters in the regulator so as to reproduce the sound velocity inferred from the observed data of neutron stars and pressure determined by the experiment of heavy-ion collisions (HICs) at high energy, i.e. we take $\nu = 2.0$ and $w = 0.4$ GeV. By choosing the large values of the parameters, the rapid rise of the momenta beyond ρ_{sat} can be completely eliminated.

Using Eqs. (23) and (24) with k_b^* and k_s^* , the total energy per nucleon in matter is given

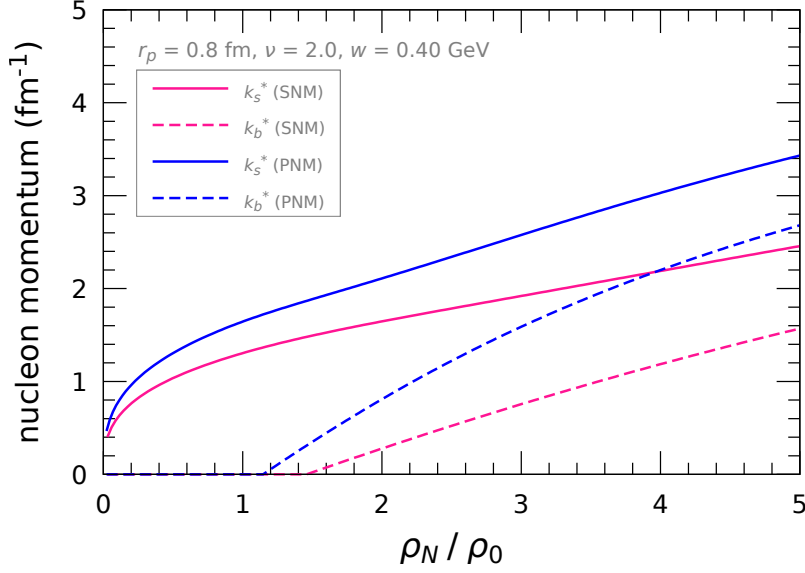


FIG. 12. Density dependence of k_s^* and k_b^* in the case of $r_p = 0.8$ fm. We take $\nu = 2.0$ and $w = 0.4$ GeV.

by Eq. (69) with

$$\epsilon_N^* = \frac{2}{\pi^2} [I(M_N^*, k_s^*) - \beta I(M_N^*, k_b^*)] \quad \text{for SNM}, \quad (81)$$

$$\epsilon_N^* = \frac{1}{\pi^2} [I(M_N^*, k_s^*) - \beta' I(M_N^*, k_b^*)] \quad \text{for PNM}. \quad (82)$$

For the mean-field of the σ meson, Eq. (71) turns out to be

$$(m_\sigma^2 + g_2 \bar{\sigma}) \bar{\sigma} = g_\sigma G_\sigma(\bar{\sigma}) \left(\frac{2M_N^*}{\pi^2} \right) [J(M_N^*, k_s^*) - \beta J(M_N^*, k_b^*)] \quad \text{for SNM}, \quad (83)$$

$$(m_\sigma^2 + g_2 \bar{\sigma}) \bar{\sigma} = g_\sigma G_\sigma(\bar{\sigma}) \left(\frac{M_N^*}{\pi^2} \right) [J(M_N^*, k_s^*) - \beta' J(M_N^*, k_b^*)] \quad \text{for PNM}. \quad (84)$$

The mean-field of ω meson in SNM is calculated by Eq. (72), in which ρ_N is given by Eq. (28) with k_b^* and k_s^* , instead of k_b and k_s . In case of PNM, the value of $\bar{\omega}$ is evaluated similarly, using Eq. (54) with k_b^* and k_s^* . In contrast, the mean-field of ρ meson in SNM vanishes because $\rho_3 = 0$, while, in PNM, it is calculated by Eq. (73), where ρ_3 is given by Eq. (54) with k_b^* and k_s^* .

Together with the results of the QMC model, the binding energy per nucleon, pressure, the mean-field value for the σ meson, the density dependences of the effective quark mass and the effective nucleon mass, and the scalar polarizability in the QQMC model are respectively

illustrated in Figs. 8, 9, 10 and 11. We note that the difference between those quantities in the QMC and QQMC models is small.

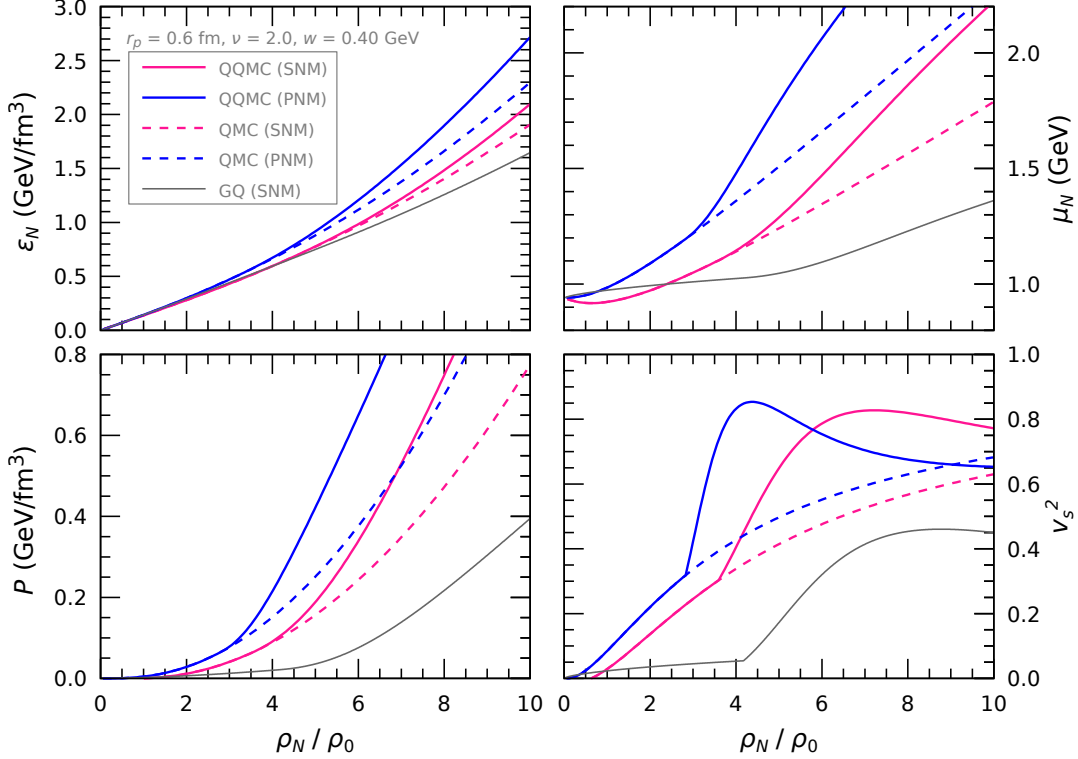


FIG. 13. Energy density, chemical potential, pressure and sound velocity in the case of $r_p = 0.6$ fm, $\nu = 2.0$ and $w = 0.4$ GeV. For comparison, we also show the result of the GQ model by the light gray curve.

Once we obtain the total energy density, ϵ_{tot} , as a function of the nuclear density, ρ_N , we can calculate the chemical potential, pressure, and sound velocity numerically by

$$\mu_N = \frac{\partial \epsilon_{tot}}{\partial \rho_N}, \quad P = \mu_N \rho_N - \epsilon_{tot}, \quad v_s^2 = \frac{\rho_N}{\mu_N} \frac{\partial \mu_N}{\partial \rho_N} = \frac{\rho_N}{\mu_N} \frac{\partial^2 \epsilon_{tot}}{\partial \rho_N^2}. \quad (85)$$

Figs. 13 and 14 present the results of the QQMC and QMC models in the case of $r_p = 0.6$ or 0.8 fm, respectively. For comparison, we add the result of the GQ model (see Sec. II C), which do not involve any nuclear interactions except for the Pauli blocking, to the figures. It is seen that the nuclear interaction is very important to describe the properties of nuclear matter quantitatively, and that, as expected, the effect of Pauli blocking at the quark level enhances the chemical potential, pressure and the sound velocity beyond ρ_{sat} .

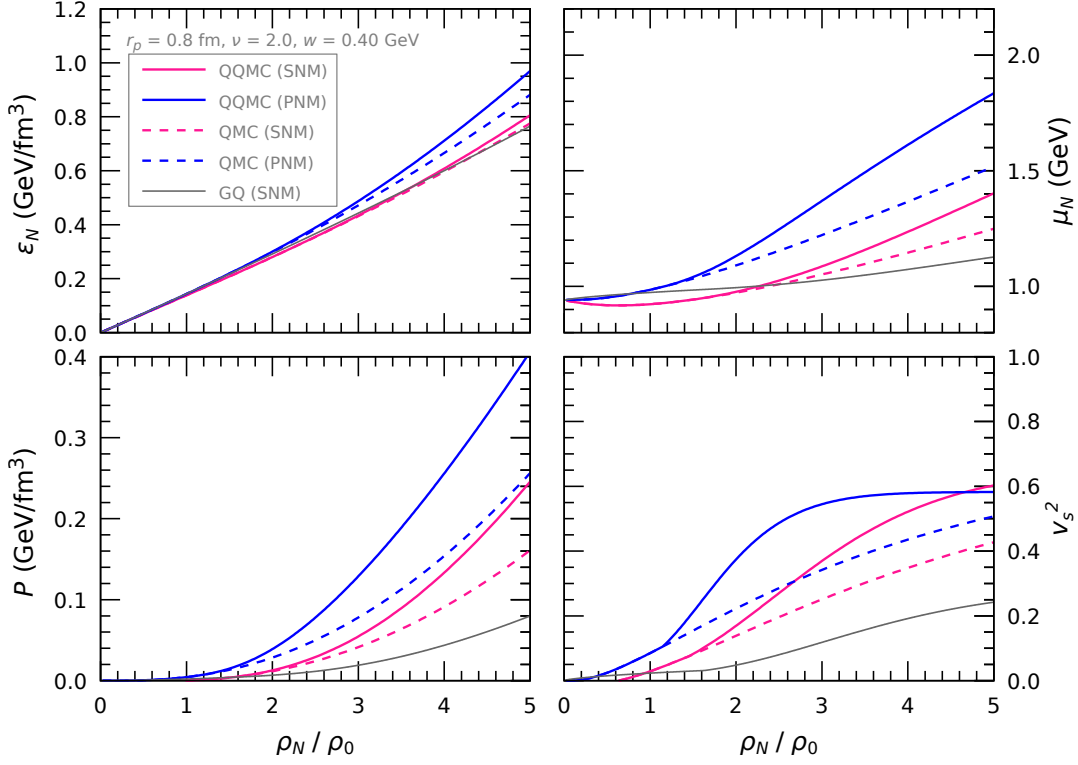


FIG. 14. Same as in Fig. 13, but for the case of $r_p = 0.8$ fm.

As for the sound velocity, it strongly depends on the nucleon size. The density dependence of v_s^2 is deduced from several neutron-star data by using the neural network model [67], in which v_s^2 shows the characteristic feature, i.e. it increases rapidly around $\rho_N/\rho_0 \sim 4.0$ and reaches the maximum ($v_s^2 \sim 0.5 - 0.8$), and then it decreases gradually beyond that density. However, such behavior can not be explained by the QMC model, in which v_s^2 grows up monotonously with increasing ρ_N . In contrast, in the case of the QQMC model with $r_p = 0.6$ fm (see Fig. 13), v_s^2 in PNM reaches the maximum, at which its value exceeds 0.8, around $\rho_N/\rho_0 \sim 4.0$, and then decreases gradually. Because a neutron star is composed of neutrons with a fraction of protons, it can be expected that the maximum value of v_s^2 in neutron-star matter turns out to be slightly smaller than the value in PNM. Thus, the sound velocity calculated by the QQMC model seems consistent with the result of v_s^2 inferred from the observed neutron-star data.

On the other hand, in Refs. [16, 68], the chemical potential, pressure, and sound velocity are extracted from Bayesian inference analysis of the observed data of neutron stars. Then, the analysis tells us that the sound velocity behaves differently than in Ref. [67], and that

it is enhanced rapidly around $\rho_N/\rho_0 \sim 2.0 - 3.0$, reaches the maximum ($v_s^2 \sim 0.6$) and is saturated beyond $\rho_N/\rho_0 \sim 3.0$. This is very close to the present result with $r_p = 0.8$ fm in PNM (see Fig. 14). Furthermore, such behavior can be explained by the OMEG family [15, 66], particularly the set of OMEG1, in relativistic mean-field theory as well.

Therefore, in the QQMC model, the value of r_p should be within the range of $0.6 - 0.8$ fm.

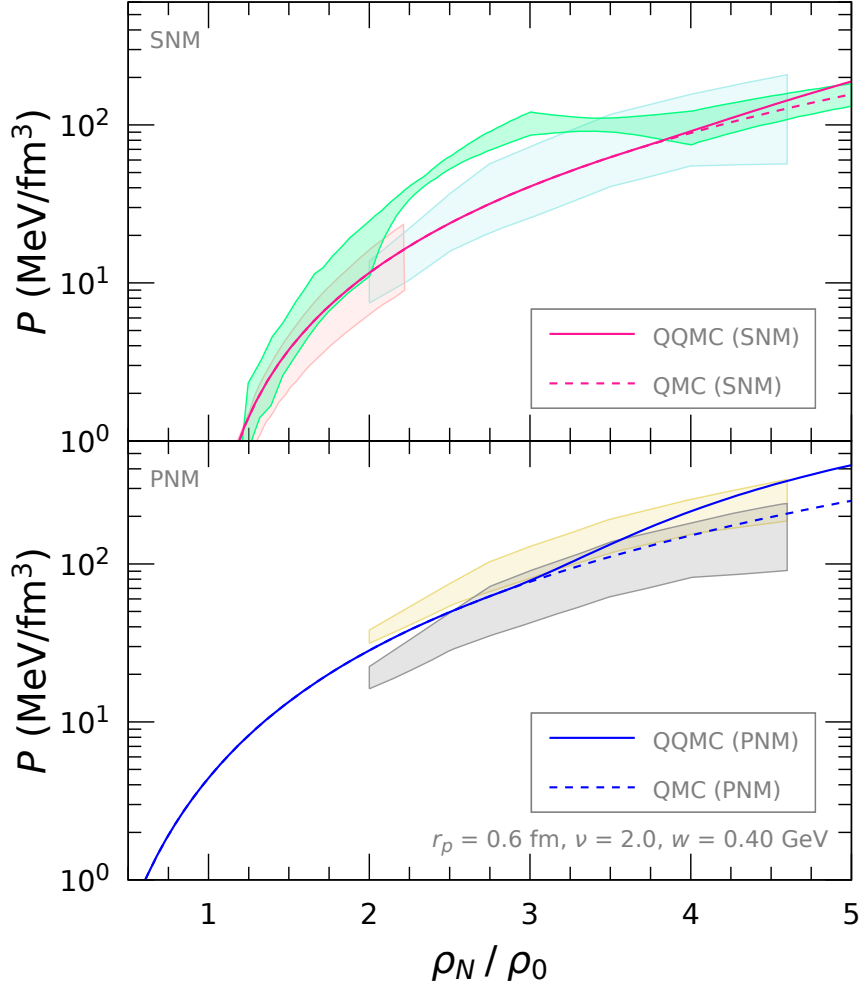


FIG. 15. Pressure in SNM or PNM as a function of ρ_N/ρ_0 . We take $r_p = 0.6$ fm, $\nu = 2.0$ and $w = 0.4$ GeV. For details, see the text.

Furthermore, we can compare the present results with the experimental data of pressure extracted from HICs at high energy. Figs. 15 and 16 show such comparisons. In the figures, the shaded areas represent the constraints from elliptical flow data [69, 70] and kaon production data [71, 72]. In both cases of $r_p = 0.6$ and 0.8 fm, pressure calculated by the QQMC or

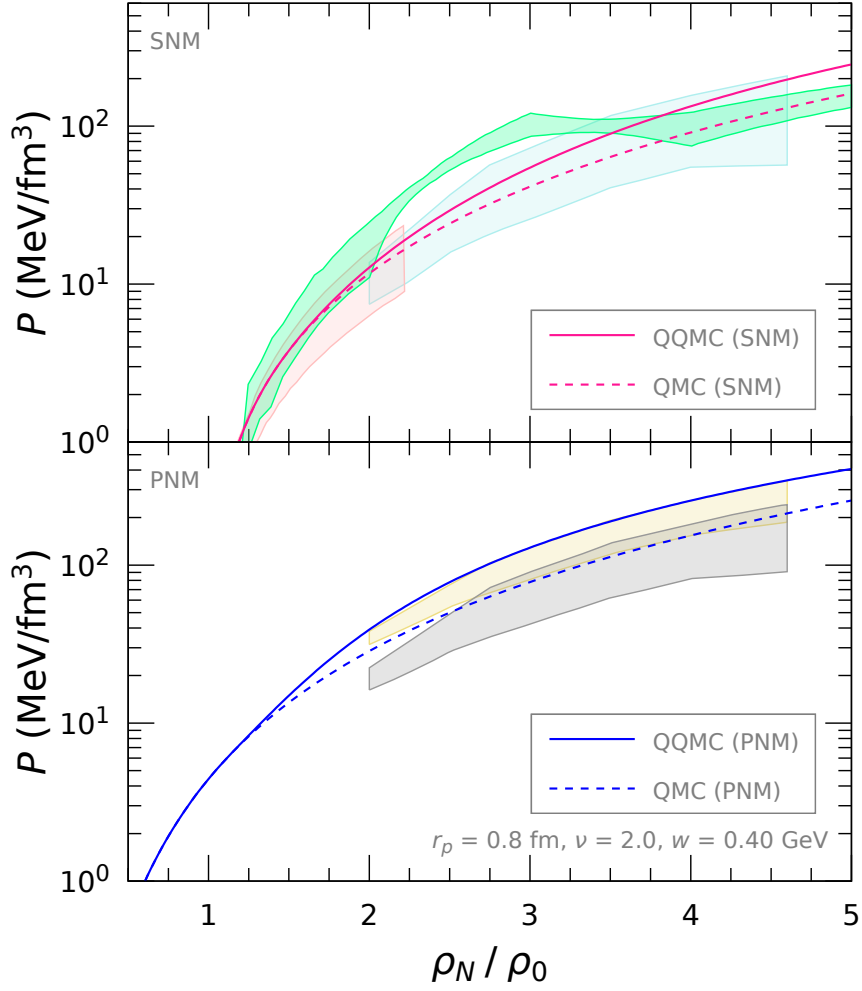


FIG. 16. Same as in Fig. 15 but for $r_\rho = 0.8 \text{ fm}$, $\nu = 2.0$ and $w = 0.4 \text{ GeV}$. For details, see the text.

QMC model is consistent with the experimental constraints. We note that pressure at high density is mainly generated by the repulsive force due to the exchanges of ω and ρ mesons, and that the effect of quarkyonic phase contributes to pressure additionally.

IV. SUMMARY AND DISCUSSION

We have constructed a novel, practical nuclear model based on the quark degrees of freedom, namely the quarkyonic quark-meson coupling (QQMC) model, in which not only the variation of nucleon structure, i.e the scalar polarizability, but also the effect of Pauli blocking at the quark level are taken into account. In the QQMC model, a relativistic, gaussian quark wavefunction is adopted to describe the structure of nucleon.

We summarize the present study as follows:

1. The quark saturation density, ρ_{sat} , is very sensitive to the quark wavefunction. In the present calculation, we have chosen the relativistic gaussian wavefunction, and, due to the lower component of the wavefunction, the value of ρ_{sat} turns out to be higher than that in the NR case. Furthermore, it is also important to consider the c.m. correction to the estimate of a nucleon radius properly. For example, in the case of the ideal (SNM) Fermi gas with $r_p = 0.8$ fm, we found that $\rho_{sat} = 1.63\rho_0$, which is higher than in the NR case by about 28%. In contrast, when the nuclear interaction is included, the quark saturation density is reduced because the nucleon size is swollen in matter. In case of $r_p = 0.8$ fm in SNM, we found that $\rho_{sat}^* = 1.46\rho_0$, which is lower than the value of 1.63 by about 10%. Thus, the quark saturation density in SNM becomes eventually larger by about 15%, compared with the value in the NR case. We note that ρ_{sat}^* in PNM is roughly 22% lower than that in SNM. In the present calculation, ρ_{sat}^* is larger than ρ_0 when $r_p \leq 0.9$ fm in SNM, while, if $r_p = 1.0$ fm, the quarkyonic phase might exist even in normal nuclei. Although in the present paper we have not studied the case of $r_p = 1.0$ fm in detail, it is certainly interesting to examine such possibility [27, 28, 31].
2. The quarkyonic phase is characterized by two momenta, k_b and k_s , where the former defines the under-occupied bulk part at low density and the latter gives the upper bound of the shell structure at high density. In the present paper, to determine those two momenta, we have used the same boundary condition as in the IdylliQ model. Then, using the gaussian quark wavefunction, we have first evaluated the energy density, chemical potential, pressure and sound velocity within the ideal Fermi gas picture. In this naïve GQ model, the chemical potential and pressure are discontinuous and the

sound velocity diverges at ρ_{sat} . To remedy this singular behavior, we have adopted the regulator which smears the sharp Fermi surface, $\theta(k_b - k)$, in the nucleon momentum distribution. Then, optimizing the regulator, we have found that the chemical potential and pressure are smoothened at ρ_{sat} , and the sound velocity becomes continuous at ρ_{sat} .

3. We have next combined the GQ model and the QMC model in order to introduce the nuclear interaction – it is called the QQMC model. The QQMC model is a nuclear model based on the quark degrees of freedom, and it is available to use over a wide range of nuclear density from low density to a crossover region where the transition from baryonic to quark matter occurs. The new model includes quarkyonic phase as well as the scalar polarizability of a nucleon in nuclear medium. We here note that, in the QQMC model, the quarks in quarkyonic phase feel the scalar field condensed in vacuum as well as are subject to the Pauli exclusion principle. Then, optimizing the regulator again, we can calculate the physical quantities, which includes the effect of nuclear interaction.
4. It is notable that the inclusion of nuclear interaction in the quarkyonic model is quite important to consider the physical quantities quantitatively. In fact, the QQMC model can provide the sound velocity which is consistent with that inferred from the observed neutron-star data by using the neural network model or Bayesian inference analysis. Furthermore, pressure in PNM or SNM calculated with the QQMC model is within the range deduced from the experiments of HICs at high energy. As the quark saturation density heavily relies on the size of nucleon, various physical quantities also depend on it accordingly. From the consideration on the sound velocity, the choice of $r_p = 0.6-0.8$ fm seems most suitable for describing dense nuclear matter in the QQMC model.

There are still some problems left. The first one concerns the boundary condition to determine the two momenta, k_b and k_s . Although in the present study we have assumed the condition which is the same as in the IdylliQ model, we need further investigation to make sure whether such condition is *sufficient* or not. At the same time, it is also necessary to find a general rule for constructing the quark momentum distribution, $f_Q(q)$, in the postsaturation region, which satisfies Fermi statistics and the minimization of energy. The second one relates to the singular behavior of physical quantities around the quark saturation density.

In the present calculation, we have used the regulator to remove it. However, basically, such singular behavior should instead be resolved by the fundamental dynamics, i.e. QCD – for example, see Refs. [73, 74]. Those are the future issues.

Finally, it may be possible to include temperature in the QQMC model and to apply the model to the EoS for neutron stars with hyperons [25, 75].

ACKNOWLEDGMENTS

K. S. thanks Yuki Fujimoto for valuable discussions on Quarkyonic matter. This work was supported by the Basic Science Research Program through the National Research Foundation of Korea (NRF) under Grant Nos. RS-2025-16071941, RS-2023-00242196, and RS-2021-NR060129.

Appendix A: Sommerfeld expansion for a gaussian quarkyonic model

In nuclear physics, for example, the Fermi function

$$f(z) = \frac{1}{1 + e^z}, \quad z = \frac{r - R}{\delta} \quad (\text{A1})$$

with R the half-density radius and δ the surface thickness is often used to describe a shape for the radial density distribution of a nucleus. However, it is more convenient to use the symmetrized Fermi function defined by [76]

$$\begin{aligned} f_s(r, R) &\equiv f((r - R)/\delta) + f(-(r + R)/\delta) - 1 \\ &= f((r - R)/\delta) - f((r + R)/\delta) = \frac{\sinh(R/\delta)}{\cosh(r/\delta) + \cosh(R/\delta)}, \end{aligned} \quad (\text{A2})$$

where $f_s(r, R) = f_s(-r, R)$, because it can avoid some difficulties appearing in actual calculations. Here, instead of the usual Fermi function, we consider minimal corrections to the GQ model by using the symmetrized Fermi function, $f_s(r, R)$.

First, we formulate Sommerfeld expansion generally. We consider the integral

$$K[h, p] = \int_0^\infty dk h(k) f_s(k, p), \quad (\text{A3})$$

with $h(k)$ any smooth function. Defining

$$H(k) \equiv \int_0^k dk' h(k'), \quad H(0) = 0, \quad (\text{A4})$$

we integrate Eq. (A3) by parts, so that

$$\begin{aligned} K[h, p] &= - \int_0^\infty dk H(k) \frac{\partial}{\partial k} f_s(k, p) = - \int_0^\infty dk H(k) \frac{\partial}{\partial k} [f(x - y) - f(x + y)], \\ &= - \int_0^\infty dk H(k) \left[\frac{\partial u}{\partial k} f'(u) - \frac{\partial v}{\partial k} f'(v) \right] = - \frac{1}{\delta} \int_0^\infty dk H(k) [f'(u) - f'(v)], \end{aligned} \quad (\text{A5})$$

with $x = k/\delta$, $y = p/\delta$, $u = x - y = (k - p)/\delta$ and $v = x + y = (k + p)/\delta$. Then, $H(k)$ is expanded around $k = p$ up to $\mathcal{O}((k - p)^2)$

$$H(k) \simeq H(p) + \delta u h(p) + \frac{1}{2} \delta^2 u^2 h'(p), \quad (\text{A6})$$

with $h'(p) = \frac{d}{dk} h(k)|_{k=p}$. Thus, we find

$$\begin{aligned} K[h, p] &\simeq -\frac{1}{\delta} H(p) \int_0^\infty dk [f'(u) - f'(v)] - h(p) \int_0^\infty dk u [f'(u) - f'(v)] \\ &\quad - \frac{\delta}{2} h'(p) \int_0^\infty dk u^2 [f'(u) - f'(v)], \end{aligned} \quad (\text{A7})$$

where the integrals in the right-hand side are evaluated as

$$\chi_0^-(y) \equiv -\frac{1}{\delta} \int_0^\infty dk [f'(u) - f'(v)] = f_s(0, y) = \tanh\left(\frac{y}{2}\right), \quad (\text{A8})$$

$$\chi_1^-(y) \equiv -\frac{1}{\delta} \int_0^\infty dk u [f'(u) - f'(v)] = \frac{2y}{1 + e^y}, \quad (\text{A9})$$

$$\chi_2^-(y) \equiv -\frac{1}{\delta} \int_0^\infty dk u^2 [f'(u) - f'(v)] = \frac{\pi^2}{3} S_2(y) + 4y \log(1 + e^{-y}), \quad (\text{A10})$$

with

$$S_2(y) \equiv \frac{12}{\pi^2} \int_0^{y/2} dt \frac{t^2}{\cosh^2 t} \simeq \frac{y^3}{y^3 + (19y^2 - 17y + 40)e^{-0.6y}} \quad (0 \leq S_2(y) \leq 1). \quad (\text{A11})$$

Note that, because of the symmetrized Fermi function, the integrals (except S_2) can be performed without any approximation. Eventually, up to $\mathcal{O}(\delta^2)$, Sommerfeld expansion gives

$$K[h, p] \simeq \chi_0^-(y) H(p) + \delta \chi_1^-(y) h(p) + \frac{1}{2} \delta^2 \chi_2^-(y) h'(p). \quad (\text{A12})$$

Similarly, we can find the first and second derivatives of $K[h, p]$ up to $\mathcal{O}(\delta^2)$ as

$$\frac{\partial}{\partial p} K[h, p] \simeq h(p) + \delta \chi_1^+(y) h'(p) + \frac{1}{2} \delta^2 \chi_2^+(y) h''(p), \quad (\text{A13})$$

with

$$\chi_1^+(y) \equiv -\frac{1}{\delta} \int_0^\infty dk u [f'(u) + f'(v)] = 2 \log(1 + e^{-y}), \quad (\text{A14})$$

$$\chi_2^+(y) \equiv -\frac{1}{\delta} \int_0^\infty dk u^2 [f'(u) + f'(v)] = \frac{\pi^2}{3} - 4y \log(1 + e^{-y}), \quad (\text{A15})$$

and

$$\frac{\partial^2}{\partial p^2} K[h, p] \simeq \chi_0^-(y) h'(p) + \delta \chi_1^-(y) h''(p) + \frac{1}{2} \delta^2 \chi_2^-(y) h'''(p). \quad (\text{A16})$$

Next, using the formula, Eqs. (A12), (A13) and (A16), we consider the minimal corrections to the GQ model, that is, we want to modify the first and seconde derivatives, $\partial k_b / \partial k_s$ and $\partial^2 k_b / \partial k_s^2$, in the naïve GQ model so as to remove the singular behavior at the quark saturation density. Here, we focus on the case of SNM only. The PNM case can be handled similarly as well.

In the boundary conditions, Eq. (25), we replace $g_Q(k_b)$ with $K[h, p]$. In Eq. (A12), in the limit $\delta \rightarrow 0$, $K[h, p]$ approaches $H(p)$, so that we set $p \rightarrow k_b$, $H \rightarrow g_Q(k_b)$ and $h \rightarrow \phi$ (see Eq. (32)). Therefore, the boundary condition with the corrections reads

$$g_Q(k_s) - \beta K[\phi, k_b] = 1, \quad (\text{A17})$$

and

$$K[\phi, k_b] \simeq \chi_0^-(k_b/\delta)g_Q(k_b) + \bar{\delta}\chi_1^-(k_b/\delta)\phi(k_b) + \frac{1}{2}\bar{\delta}^2\chi_2^-(k_b/\delta)\phi'(k_b), \quad (\text{A18})$$

where $\bar{\delta} = a\delta/N_c$ is dimensionless and ϕ' is given by Eq. (46). Fig. 17 depicts the momenta, k_b and k_s , calculated with Sommerfeld expansion, Eq. (A17). We can see that the rapid rise of the momenta appeared in the naïve GQ model is softened at ρ_{sat} .

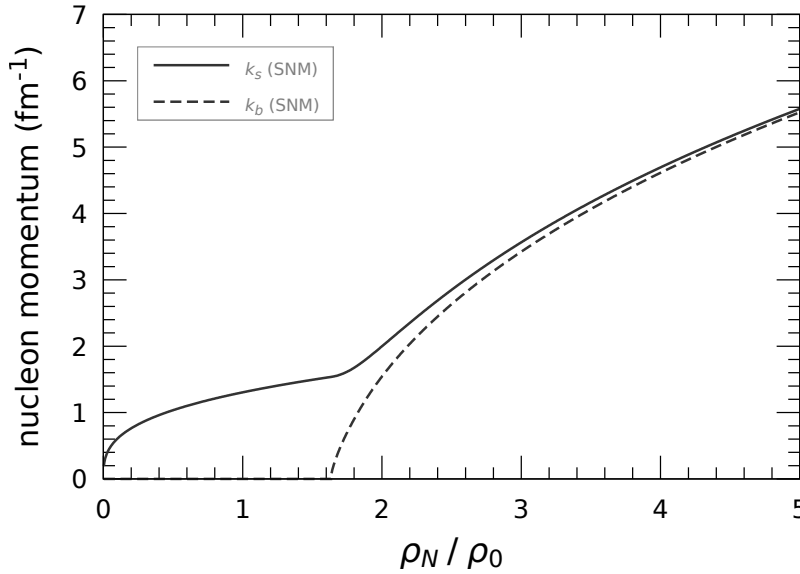


FIG. 17. Momenta, k_s and k_b , in Sommerfeld expansion. We choose $w = 35$ MeV in the case of $r_p = 0.8$ fm.

Furthermore, the first derivative of $K[\phi, k_b]$ with respect to \bar{k}_b is given by Eq. (A13)

$$\frac{\partial K[\phi, k_b]}{\partial \bar{k}_b} \simeq \phi(k_b) + \bar{\delta}\chi_1^+(k_b/\delta)\phi'(k_b) + \frac{1}{2}\bar{\delta}^2\chi_2^+(k_b/\delta)\phi''(k_b). \quad (\text{A19})$$

Thus, we obtain the first derivative, $\partial k_b/\partial k_s$, as

$$\begin{aligned} \frac{\partial k_b}{\partial k_s} &= \frac{\partial \bar{k}_b}{\partial k_s} \\ &= \frac{\phi(k_s)}{\beta[\phi(k_b) + \bar{\delta}\chi_1^+(k_b/\delta)\phi'(k_b) + \frac{1}{2}\bar{\delta}^2\chi_2^+(k_b/\delta)\phi''(k_b)]}, \end{aligned} \quad (\text{A20})$$

with

$$\phi''(k) = \frac{N_c^3}{\sqrt{\pi}} 8[r_1(k) - 5r_2(k)\bar{k}^2 + 2r_3(k)\bar{k}^4]e^{-\bar{k}^2}. \quad (\text{A21})$$

We notice that, as $k_b \rightarrow 0$, the denominator in Eq. (A20) is $\mathcal{O}(1)$ and thus the singular behavior at ρ_{sat} vanishes.

To calculate the sound velocity, we need the second derivative, $\partial^2 k_b/\partial k_s^2$, which should be modified as well. Using Eqs. (A16), (A17), and (A20), we find

$$\frac{\partial^2 \bar{k}_b}{\partial \bar{k}_s^2} = \left(\frac{N_c}{a}\right) \frac{\partial^2 k_b}{\partial k_s^2} = \frac{\phi'(k_s) - \beta \left(\frac{\partial \bar{k}_b}{\partial k_s}\right)^2 \frac{\partial^2}{\partial \bar{k}_b^2} K[\phi, k_b]}{\beta[\phi(k_b) + \bar{\delta}\chi_1^+(k_b/\delta)\phi'(k_b) + \frac{1}{2}\bar{\delta}^2\chi_2^+(k_b/\delta)\phi''(k_b)]}, \quad (\text{A22})$$

with

$$\frac{\partial^2}{\partial \bar{k}_b^2} K[\phi, k_b] \simeq \chi_0^-(k_b/\delta)\phi'(k_b) + \bar{\delta}\chi_1^-(k_b/\delta)\phi''(k_b) + \frac{1}{2}\bar{\delta}^2\chi_2^-(k_b/\delta)\phi'''(k_b), \quad (\text{A23})$$

and

$$\phi'''(k) = \frac{N_c^3}{\sqrt{\pi}} (-16)\bar{k}[6r_2(k) - 9r_3(k)\bar{k}^2 + 2r_4(k)\bar{k}^4]e^{-\bar{k}^2}. \quad (\text{A24})$$

We again notice that the denominator in Eq. (A22) is $\mathcal{O}(1)$ as $k_b \rightarrow 0$.

Now, all we need is prepared. Along the line of Section II B, we can calculate ρ_N , ϵ_N , μ_N , P , and v_s^2 by using Eqs. (A20) and (A22), instead of Eqs. (31) and (45). Fig. 18 illustrates the results. We take $\delta = 35$ MeV and $r_p = 0.8$ fm. All the calculated quantities are continuous at ρ_{sat} . Furthermore, the sound velocity does not diverge. However, it overshoots the upper limit. A larger value of δ can, of course, suppress the sound velocity around ρ_{sat} , but it turns out to be negative at very high density. Therefore, the present expansion up to $\mathcal{O}(\delta^2)$ may be insufficient, and we should include higher order contributions beyond $\mathcal{O}(\delta^2)$ to obtain a satisfactory result. It may be very intricate.

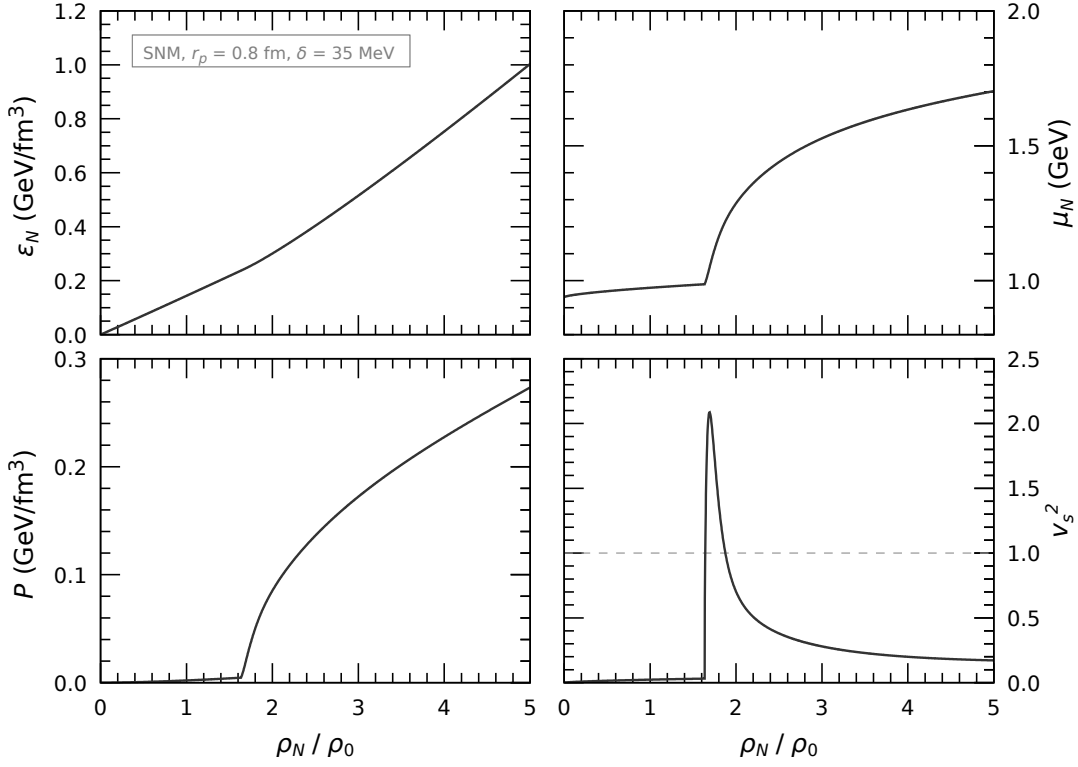


FIG. 18. Energy density, chemical potential, pressure, and sound velocity in Sommerfeld expansion.

-
- [1] B. P. Abbott *et al.* (LIGO Scientific, Virgo), Phys. Rev. Lett. **119**, 161101 (2017), arXiv:1710.05832 [gr-qc].
 - [2] B. P. Abbott *et al.* (LIGO Scientific, Virgo), Phys. Rev. X **9**, 011001 (2019), arXiv:1805.11579 [gr-qc].
 - [3] B. P. Abbott *et al.* (LIGO Scientific, Virgo), Phys. Rev. Lett. **121**, 161101 (2018), arXiv:1805.11581 [gr-qc].
 - [4] Z. Arzoumanian *et al.* (NANOGrav), Astrophys. J. Suppl. **235**, 37 (2018), arXiv:1801.01837 [astro-ph.HE].
 - [5] P. Demorest, T. Pennucci, S. Ransom, M. Roberts, and J. Hessels, Nature **467**, 1081 (2010), arXiv:1010.5788 [astro-ph.HE].
 - [6] J. Antoniadis *et al.*, Science **340**, 6131 (2013), arXiv:1304.6875 [astro-ph.HE].

- [7] E. Fonseca *et al.*, *Astrophys. J. Lett.* **915**, L12 (2021), arXiv:2104.00880 [astro-ph.HE].
- [8] R. W. Romani, D. Kandel, A. V. Filippenko, T. G. Brink, and W. Zheng, *Astrophys. J. Lett.* **934**, L17 (2022), arXiv:2207.05124 [astro-ph.HE].
- [9] S. Vinciguerra *et al.*, *Astrophys. J.* **961**, 62 (2024), arXiv:2308.09469 [astro-ph.HE].
- [10] D. Choudhury *et al.*, *Astrophys. J. Lett.* **971**, L20 (2024), arXiv:2407.06789 [astro-ph.HE].
- [11] T. Salmi *et al.*, *Astrophys. J.* **974**, 294 (2024), arXiv:2406.14466 [astro-ph.HE].
- [12] T. Salmi *et al.*, *Astrophys. J.* **976**, 58 (2024), arXiv:2409.14923 [astro-ph.HE].
- [13] L. Mauviard *et al.*, arXiv:2506.14883 [astro-ph.HE].
- [14] A. Li *et al.*, *Sci. China Phys. Mech. Astron.* **68**, 119503 (2025), arXiv:2506.08104 [astro-ph.HE].
- [15] T. Miyatsu, M.-K. Cheoun, K. Kim, and K. Saito, *Front. in Phys.* **12**, 1531475 (2024), arXiv:2411.13210 [nucl-th].
- [16] L. Brandes and W. Weise, *Symmetry* **16**, 111 (2024), arXiv:2312.11937 [nucl-th].
- [17] T. Miyatsu, M.-K. Cheoun, K. Kim, and K. Saito, *Symmetry* **17**, 1872 (2025), arXiv:2509.16559 [nucl-th].
- [18] L. McLerran and R. D. Pisarski, *Nucl. Phys. A* **796**, 83 (2007), arXiv:0706.2191 [hep-ph].
- [19] G. Baym, T. Hatsuda, T. Kojo, P. D. Powell, Y. Song, and T. Takatsuka, *Rept. Prog. Phys.* **81**, 056902 (2018), arXiv:1707.04966 [astro-ph.HE].
- [20] K. Fukushima, T. Kojo, and W. Weise, *Phys. Rev. D* **102**, 096017 (2020), arXiv:2008.08436 [hep-ph].
- [21] T. Kojo, *J. Subatomic Part. Cosmol.* **4**, 100088 (2025), arXiv:2412.20442 [nucl-th].
- [22] O. Ivanytskyi, *Phys. Rev. D* **112**, 034001 (2025), arXiv:2505.07076 [nucl-th].
- [23] C. Gärtlein, O. Ivanytskyi, V. Sagun, and I. Lopes, arXiv:2509.03517 [nucl-th].
- [24] Y. Fujimoto, T. Kojo, and L. D. McLerran, *Phys. Rev. Lett.* **132**, 112701 (2024), arXiv:2306.04304 [nucl-th].
- [25] Y. Fujimoto, T. Kojo, and L. McLerran, arXiv:2410.22758 [nucl-th].
- [26] V. Koch and V. Vovchenko, *J. Subatomic Part. Cosmol.* **3**, 100025 (2025).
- [27] V. Koch, L. McLerran, G. A. Miller, and V. Vovchenko, *Phys. Rev. C* **110**, 025201 (2024), arXiv:2403.15375 [nucl-th].
- [28] L. McLerran and G. A. Miller, *Phys. Rev. C* **110**, 045203 (2024), arXiv:2405.11074 [nucl-th].
- [29] D. F. Geesaman, K. Saito, and A. W. Thomas, *Ann. Rev. Nucl. Part. Sci.* **45**, 337 (1995).
- [30] M. Arneodo, *Phys. Rept.* **240**, 301 (1994).

- [31] A. Nikolakopoulos and G. A. Miller, arXiv:2506.22670 [nucl-th].
- [32] K. Saito, K. Tsushima, and A. W. Thomas, Prog. Part. Nucl. Phys. **58**, 1 (2007), arXiv:hep-ph/0506314.
- [33] P. A. M. Guichon, J. R. Stone, and A. W. Thomas, Prog. Part. Nucl. Phys. **100**, 262 (2018), arXiv:1802.08368 [nucl-th].
- [34] G. Krein, A. W. Thomas, and K. Tsushima, Prog. Part. Nucl. Phys. **100**, 161 (2018), arXiv:1706.02688 [hep-ph].
- [35] P. A. M. Guichon, Phys. Lett. B **200**, 235 (1988).
- [36] K. Saito and A. W. Thomas, Phys. Lett. B **327**, 9 (1994), arXiv:nucl-th/9403015.
- [37] P. A. M. Guichon, K. Saito, E. N. Rodionov, and A. W. Thomas, Nucl. Phys. A **601**, 349 (1996), arXiv:nucl-th/9509034.
- [38] K. Saito and K. Tsushima, Prog. Theor. Phys. **105**, 373 (2001), arXiv:nucl-th/0012090.
- [39] K. Saito, K. Tsushima, and A. W. Thomas, Phys. Lett. B **406**, 287 (1997), arXiv:nucl-th/9704047.
- [40] K. Tsushima, K. Saito, and A. W. Thomas, Phys. Lett. B **411**, 9 (1997), [Erratum: Phys.Lett.B 421, 413 (1998)], arXiv:nucl-th/9701047.
- [41] P. A. M. Guichon, A. W. Thomas, and K. Tsushima, Nucl. Phys. A **814**, 66 (2008), arXiv:0712.1925 [nucl-th].
- [42] D.-H. Lu, A. W. Thomas, K. Tsushima, A. G. Williams, and K. Saito, Phys. Lett. B **417**, 217 (1998), arXiv:nucl-th/9706043.
- [43] D.-H. Lu, K. Tsushima, A. W. Thomas, A. G. Williams, and K. Saito, Phys. Rev. C **60**, 068201 (1999), arXiv:nucl-th/9807074.
- [44] T. Kolar *et al.* (A1), Phys. Rev. C **110**, L061302 (2024), arXiv:2311.01935 [nucl-ex].
- [45] K. Saito and A. W. Thomas, Nucl. Phys. A **574**, 659 (1994).
- [46] I. C. Cloet, W. Bentz, and A. W. Thomas, Phys. Lett. B **642**, 210 (2006), arXiv:nucl-th/0605061.
- [47] A. W. Thomas, P. A. M. Guichon, D. B. Leinweber, and R. D. Young, Prog. Theor. Phys. Suppl. **156**, 124 (2004), arXiv:nucl-th/0411014.
- [48] E. Chang, Z. Davoudi, W. Detmold, A. S. Gambhir, K. Orginos, M. J. Savage, P. E. Shanahan, M. L. Wagman, and F. Winter (NPLQCD), Phys. Rev. Lett. **120**, 152002 (2018), arXiv:1712.03221 [hep-lat].

- [49] T. Katayama, T. Miyatsu, and K. Saito, *Astrophys. J. Suppl.* **203**, 22 (2012), arXiv:1207.1554 [astro-ph.SR].
- [50] T. Miyatsu, T. Katayama, and K. Saito, *Phys. Lett. B* **709**, 242 (2012), arXiv:1110.3868 [nucl-th].
- [51] T. Miyatsu, M.-K. Cheoun, and K. Saito, *Astrophys. J.* **813**, 135 (2015), arXiv:1506.05552 [nucl-th].
- [52] D. H. Rischke, M. I. Gorenstein, H. Stoecker, and W. Greiner, *Z. Phys. C* **51**, 485 (1991).
- [53] J. Leong, A. W. Thomas, and P. A. M. Guichon, *Nucl. Phys. A* **1050**, 122928 (2024), arXiv:2308.08987 [nucl-th].
- [54] W. Bentz and I. C. Cloët, *Symmetry* **17**, 505 (2025), arXiv:2503.20564 [nucl-th].
- [55] H. Toki, U. Meyer, A. Faessler, and R. Brockmann, *Phys. Rev. C* **58**, 3749 (1998).
- [56] H. Shen and H. Toki, *Phys. Rev. C* **61**, 045205 (2000), arXiv:nucl-th/9911046.
- [57] N. Barik, R. N. Mishra, D. K. Mohanty, P. K. Panda, and T. Frederico, *Phys. Rev. C* **88**, 015206 (2013), arXiv:1307.0934 [nucl-th].
- [58] K. Saito, T. Miyatsu, and M.-K. Cheoun, *Phys. Rev. D* **110**, 113001 (2024), arXiv:2409.14764 [hep-ph].
- [59] P. Leal Ferreira, *Lett. Nuovo Cim.* **20**, 157 (1977).
- [60] P. Leal Ferreira and N. Zagury, *Lett. Nuovo Cim.* **20**, 511 (1977).
- [61] N. Barik and B. K. Dash, *Phys. Rev. D* **33**, 1925 (1986).
- [62] Z. Zhu, A. Li, J. Hu, and H. Shen, *Phys. Rev. C* **108**, 025809 (2023), arXiv:2305.16058 [nucl-th].
- [63] S. Navas *et al.* (Particle Data Group), *Phys. Rev. D* **110**, 030001 (2024).
- [64] T. Kojo, *Phys. Rev. D* **104**, 074005 (2021), arXiv:2106.06687 [nucl-th].
- [65] T. Miyatsu, M.-K. Cheoun, and K. Saito, *Astrophys. J.* **929**, 82 (2022), arXiv:2202.06468 [nucl-th].
- [66] T. Miyatsu, M.-K. Cheoun, K. Kim, and K. Saito, *Phys. Lett. B* **843**, 138013 (2023), arXiv:2303.14763 [nucl-th].
- [67] Y. Fujimoto, K. Fukushima, and K. Murase, *Phys. Rev. D* **101**, 054016 (2020), arXiv:1903.03400 [nucl-th].
- [68] L. Brandes and W. Weise, *Phys. Rev. D* **111**, 034005 (2025), arXiv:2412.05923 [nucl-th].
- [69] P. Danielewicz, R. Lacey, and W. G. Lynch, *Science* **298**, 1592 (2002), arXiv:nucl-th/0208016.

- [70] D. Oliinychenko, A. Sorensen, V. Koch, and L. McLerran, Phys. Rev. C **108**, 034908 (2023), arXiv:2208.11996 [nucl-th].
- [71] C. Fuchs, Prog. Part. Nucl. Phys. **56**, 1 (2006), arXiv:nucl-th/0507017.
- [72] W. G. Lynch, M. B. Tsang, Y. Zhang, P. Danielewicz, M. Famiano, Z. Li, and A. W. Steiner, Prog. Part. Nucl. Phys. **62**, 427 (2009), arXiv:0901.0412 [nucl-ex].
- [73] T. Kojo and D. Suenaga, Phys. Rev. D **105**, 076001 (2022), arXiv:2110.02100 [hep-ph].
- [74] H. Tajima, K. Iida, T. Kojo, and H. Liang, Phys. Rev. Lett. **135**, 042701 (2025), arXiv:2412.04971 [hep-ph].
- [75] M. Bluhm, Y. Fujimoto, L. McLerran, and M. Nahrgang, Phys. Rev. C **111**, 044914 (2025), arXiv:2409.12088 [nucl-th].
- [76] D. Sprung and J. Martorell, J. Phys. A Math. Gen. **30**, 6525 (1997).